Continuum Mech. Thermodyn. (2016) 28:1847–1885
DOI 10.1007/s00161-016-0511-4

ORIGINAL ARTICLE

C. Xu · M. K. Mudunuru · K. B. Nakshatrala

Material degradation due to moisture and temperature. Part 1: mathematical model, analysis, and analytical solutions

Received: 21 January 2016 / Accepted: 28 May 2016 / Published online: 30 June 2016

Abstract The mechanical response, serviceability, and load-bearing capacity of materials and structural components can be adversely affected due to external stimuli, which include exposure to a corrosive chemical species, high temperatures, temperature fluctuations (i.e., freezing–thawing), cyclic mechanical loading, just to name a few. It is, therefore, of paramount importance in several branches of engineering—ranging from aerospace engineering, civil engineering to biomedical engineering—to have a fundamental understanding of degradation of materials, as the materials in these applications are often subjected to adverse environments. As a result of recent advancements in material science, new materials such as fiber-reinforced polymers and multi-functional materials that exhibit high ductility have been developed and widely used, for example, as infrastructural materials or in medical devices (e.g., stents). The traditional small-strain approaches of modeling these materials will not be adequate. In this paper, we study degradation of materials due to an exposure to chemical species and temperature under large strain and large deformations. In the first part of our research work, we present a consistent mathematical model with firm thermodynamic underpinning. We then obtain semi-analytical solutions of several canonical problems to illustrate the nature of the quasi-static and unsteady behaviors of degrading hyperelastic solids.

Keywords Degradation · Aging · Continuum damage mechanics · Coupled chemo–thermo–mechano analysis · Semi-analytical solutions · Constitutive modeling · Hyperelasticity

List of symbols

ρ	Density of solid in deformed configuration ($\mathrm{kg\,m^{-3}}$)
A	Specific Helmholtz potential ($\mathrm{J\,kg^{-1}}$)
ζ	Dissipation functional ($\mathrm{J\,kg^{-1}\,s^{-1}}$)
ψ	Strain energy density functional ($\mathrm{J\,m^{-3}}$)
λ, μ	Lamé parameters (Pa)
κ	Bulk modulus (Pa)
$\mathbf{u}$	Displacement (m)
$\mathbf{v}$	Velocity ($\mathrm{m\,s^{-1}}$)
ϑ	Temperature (K)
c	Concentration (l)

C. Xu and M.K. Mudunuru are graduate students at University of Houston.

Communicated by Andreas Öchsner.

C. Xu · M. K. Mudunuru · K. B. Nakshatrala (✉)
Department of Civil and Environmental Engineering, University of Houston, Houston, TX 77204–4003, USA
E-mail: knakshatrala@uh.edu

R_s	Specific vapor constant ($\mathrm{J\,kg^{-1}\,K^{-1}}$)
c_p	Heat capacity ($\mathrm{J\,kg^{-1}\,K^{-1}}$)
$\mathbf{M}_{\vartheta\mathbf{E}}$	Thermal expansion tensor ($\mathrm{J\,m^{-3}\,K^{-1}}$)
$\mathbf{M}_{c\mathbf{E}}$	Chemical expansion tensor ($\mathrm{J\,m^{-3}}$)
$d_{\vartheta c}$	Thermo–chemo coupled parameter ($\mathrm{J\,kg^{-1}\,K^{-1}}$)
$\varkappa$	Specific chemical potential ($\mathrm{J\,kg^{-1}}$)
η	Specific entropy ($\mathrm{J\,kg^{-1}\,K^{-1}}$)
$\mathbf{D}_{\vartheta\vartheta}$	Thermal diffusion tensor ($\mathrm{m^2\,s^{-1}}$)
$\mathbf{D}_{\varkappa\varkappa}$	Diffusivity tensor ($\mathrm{m^2\,s^{-1}}$)
$\mathbf{D}_{\vartheta\varkappa}$, $\mathbf{D}_{\varkappa\vartheta}$	Dufour–Soret effect tensors ($\mathrm{m^2\,s^{-1}}$)
$\mathbf{T}$	Cauchy stress (Pa)
$\mathbf{h}$	Diffusive flux vector ($\mathrm{kg\,m^{-2}\,s^{-1}}$)
$\mathbf{q}$	Heat flux vector ($\mathrm{J\,m^{-2}\,s^{-1}}$)
h	Volumetric source ($\mathrm{kg\,m^{-3}\,s^{-1}}$)
q	Volumetric heat source ($\mathrm{J\,m^{-3}\,s^{-1}}$)

1 Introduction and motivation

Material and structural degradation is a major problem in infrastructure and various other real-life applications. Most of the well-known manifestations, such as "wear out," "fracture," "spalling," and "section loss," are related to the phenomenon of degradation [6]. Virtually, every material degrades when subjected to hostile environment and external stimuli. Importance of these phenomena has triggered a surge in research to develop more resistible materials. Consequently, understanding the general behavior of degrading materials has attracted the interest of researchers. A fundamental study of degradation is crucial to several branches of engineering: aerospace, mechanical, civil, and biomedical. Moreover, some new materials such as fiber-reinforced polymers and multi-functional materials that exhibit high ductility have been widely used recently, for example, as infrastructural materials or in medical devices (e.g., stents). In order to model these materials, the traditional small-strain assumption will not be sufficient anymore.

In a nutshell, degradation means the loss in either serviceability or functionality. To be precise, a material is said to be undergoing thermal degradation at a spatial point $\mathbf{x} \in \Omega$ if the available energy density under isothermal condition is lower than the reference available isothermal power at that particular point. That is,

$$\left.\frac{\mathrm{d}A}{\mathrm{d}t}\right|_{\vartheta>\vartheta_{\mathrm{ref}}} \leqslant \left.\frac{\mathrm{d}A}{\mathrm{d}t}\right|_{\vartheta=\vartheta_{\mathrm{ref}}} \quad \text{for } \mathbf{x} \in \Omega \tag{1.1}$$

Similarly, the chemical/moisture degradation can be defined as follows:

$$\left.\frac{\mathrm{d}A}{\mathrm{d}t}\right|_{c>c_{\mathrm{ref}}} \leqslant \left.\frac{\mathrm{d}A}{\mathrm{d}t}\right|_{c=c_{\mathrm{ref}}} \quad \text{for } \mathbf{x} \in \Omega \tag{1.2}$$

where A denotes the specific Helmholtz potential of the material, Ω is the degrading body under consideration, t is the time of interest, and ϑ_{ref} and c_{ref} are the specified reference temperature and reference concentration, respectively. Note that degradation not only reduces the durability of materials but also alters material properties. For instance, material damage can induce anisotropy in thermal conductivity and diffusivity [59,74,82].

Herein, we develop a coupled continuum mathematical model for thermal and chemical-induced degradation of solids, which are initially hyperelastic. We now outline three main reasons for such a need.

1. There is irrefutable experimental evidence that many modern infrastructural materials used in repair and retrofitting applications exhibit large deformations. For example, the popular high-early-strength engineered cementitious composites (ECC) are capable of delivering a compressive strength of 21 MPa within 4 h after placement. Moreover, the long-term tensile strain capacity of ECC members is more than 2 % [45,76].
2. In order to understand degradation mechanisms due to moisture, chemical, and temperature, coupling at various levels is needed (which is due to balance laws, material parameters, boundary conditions, and initial conditions). With existing and popular multi-physics packages such ABAQUS [1], ANSYS [4], and COMSOL [18], it is possible to couple certain degradation mechanisms to some extent at material parameters, boundary conditions, and initial conditions. However, such packages *do not offer* flexibility to couple important heat and mass transfer terms in balance laws. This is of utmost importance in capturing the effects of chemo–thermo–mechano degradation.

3. Finally, when a new model or a thermodynamic framework is developed, stability of the solutions for the corresponding initial boundary value problem needs to be shown. However, such an analysis is rarely performed when a new degradation model/framework is developed in the literature. Herein, for the proposed degradation framework we shall perform stability analysis in the sense of Lyapunov. Subsequently, this methodology shall be used to construct a robust computational framework in the part II of the paper.

Hence, due to the above reasons small-strain assumptions to model degradation and healing behavior of these infrastructural systems are rarely valid. The proposed framework takes into account the underlying degradation mechanisms. Correspondingly, the respective parameters have a physical meaning and can be calibrated through experiments.

It should be emphasized that elasticity is an idealization. There is no material whose response is perfectly elastic. But there are situations in which the response of certain materials under normal conditions can be idealized to be hyperelastic, for example, large blood arteries and rock. Many of these materials function in hostile environments and are constantly subjected to adverse external stimuli. One often is interested in the unsteady response of the bodies made of hyperelastic materials subjected to degradation/healing. The application areas in mind are the response of high-performance cementitious materials (which undergo large strains and large deformations) and several important coupled deformation–thermal-transport processes in biomechanics and biomedicine. In the next couple of subsections, we shall discuss various degradation mechanisms and the deficiencies in the existing frameworks in modeling chemo–thermo–mechano degradation.

1.1 Degradation mechanisms

There are many mechanisms that can result in the degradation of materials and structures. In general, the degradation mechanisms can be divided into four categories: mechanical processes, chemical reactions, biological degradation [29], and radiation [39]. For mechanical processes, the performance of materials can be affected adversely by fatigue [37], pressure loading [63], and swelling of solid mixtures [13]. Examples of chemical degradation include humid and alkaline effects [8], exposure to chlorides and carbon dioxide [26], and calcium leaching [25]. Biological degradation refers to the dissolution of materials by bacteria or other microorganisms. Degradation induced by radiation includes radiation damage as well as other mechanical and chemical processes triggered by radiation.

The coupling effects between these mechanisms can have a significant impact on the rate of deterioration of materials and structures. For instance, see Table 1 for some important factors that affect the degradation modeling in infrastructural materials such as concrete. Therefore, developing an appropriate and general model for material degradation is useful to predict the life span of a given structure. A comprehensive understanding of chemo–thermo–mechano degradation not only plays a pivotal role in improving the quality and reliability of existing infrastructure, but also has a tremendous impact on the economy [34]. In this paper, we shall assume that predominant degradation mechanisms are moisture and temperature. We propose a general three-way strongly coupled degradation model based on a thermodynamic framework. This three-way coupling is between mechanical, thermal, and chemical transport processes.

Table 1 Various degradation mechanics and their primary manifestation

Degradation factor	Primary manifestation
Physical processes	
Cracking	Reduced durability
Vibration	Cracking
Freezing and thawing	Cracking/scaling/disintegration
Abrasion/erosion/cavitation	Section loss
Thermal exposure/thermal cycling	Cracking/spalling/strength loss
Chemical processes	
Efflorescence/leaching	Increased porosity
Phosphate	Surface deposits
Sulfate attack	Volume change/cracking
Acids/bases	Disintegration/spalling/leaching
Alkali-aggregate reactions	Disintegration/cracking

Many other factors can be found in [55] for cementitious materials and concrete structures

1.2 Thermodynamics of chemo–thermo–mechano degradation

Herein, we shall provide a brief review and current status of thermal and chemical degradation. In the literature, thermal degradation is modeled based on variants of thermo-elasticity by incorporating damage variables. Some popular research works in this direction are [81] for modeling thermo-mechanical damage processes in heterogeneous cementitious materials and [3] on the behavior of reinforced concrete slabs exposed to fire. On the other hand, some popular research works for the chemical degradation are [8] on the environmental effects of alkalinity and humidity on concrete slabs, [16] on moisture damage mechanisms occurring within asphaltic materials and pavements, [11] on thermal and moisture effects on structural stiffness and damping of laminated composites, and [78,79] on fluid-induced damage and absorption in polymeric composites. However, none of the above-mentioned papers on thermal or chemical degradation have a proper thermodynamic basis.

There are two popular approaches to constructing thermodynamically-consistent degradation models. The first approach is based on the theory of the internal variable, wherein a scalar (or a tensor) variable is introduced to model the degree of damage [27,63,69,77]. For instance, the damage variable may represent the measure of the fraction of broken cross-links or micro-cracks in a representative volume element of the body [38,44,75]. The main disadvantage of this approach is that it may not be always possible to measure the internal variables through experiments or associate them to physical quantities/parameters. However, due to the recent advances in experimental and characterization techniques (e.g., non-destructive experimental methods [24,28] and digital image correlation techniques [61,71]) it is now possible to measure and assign physical meaning to an internal variable in some scenarios. For instance, internal variable can correspond to fracture density in a representative volume element of the body. In some very complicated problems (e.g., degradation of polymers due to oxidation), an internal approach can have a distinctive advantage. In these complicated problems, it may not be possible to include all the coupled physical and chemical processes, which can be either due to lack of current understanding of various underlying processes or due to intractability of the resulting problem. In such scenarios, the internal variable approach can offer a viable modeling approach.

The second approach is to build a thermodynamic framework by modeling all the relevant coupled processes. This achieved by taking into account the dependence of material properties on the deformation of the solid, temperature, and concentration of chemical species. The degradation parameters under this approach have physical basis and can be calibrated using experiments (e.g., see Sect. 5 of this paper). Herein, we shall employ the second approach to developing a thermodynamically-consistent degradation model. It should be noted that certain research works exist in the literature wherein the degradation models using the second approach, for example, see [21,40,41,53]. However, it appears that the above-cited works suffer from the main drawback that they considered thermodynamics of chemo–thermo–mechano degradation in the context of a closed system as opposed to an open system, which is the approach taken in this paper. For instance, $\mathrm{div}[\varkappa \mathbf{h}]$ and $\mathrm{grad}[\varkappa] \bullet \mathbf{h}$ are not taken into account in the aforementioned papers. These terms are responsible for mass transfer in balance of energy and second law of thermodynamics [see Eqs. (2.16), (2.20) in Sect. 2]. In other words, their treatment of mass transfer is pure mechanical. In strict sense, such a treatment does not fall under open system thermodynamics.

1.3 Scope of the paper

The main contributions and the scope of the paper can be enumerated as follows:

1. We derive a general chemo–thermo–mechano degradation model by appealing to the maximization of rate of dissipation. It will be shown that the proposed model can recover many popular models. For example, Fickian model, Fourier model, Dufour–Soret model, thermo-elasticity, chemoelasticity [68], chemo–thermo-elasticity [19,68], and the small-strain moisture degradation model proposed in [52] are all special cases of the proposed model.
2. We calibrate the proposed degradation model (specifically, we calibrated for deformation-dependent diffusivity) with an existing experimental data set available. The data set pertains to glass, which is a brittle material. For this calibration case, thermal effects are not considered as the data for temperature and deformation-dependent thermal conductivity is not available for glassy fibers (as per our knowledge). Such a study is straightforward, whenever deformation-dependent conductivity data set is available. This calibration study should provide confidence in employing the proposed constitutive model to model degradation of various brittle and quasi-brittle materials such as ceramics, glass fibers, and concrete.

3. A systematic mathematical analysis is presented for the proposed model under large/finite deformations. In particular, we shall show that the unsteady solutions under the proposed degradation model are bounded and are stable in the sense of Lyapunov.
4. Last but not the least, semi-analytical solutions to several canonical problems are presented, which provide insights into the behavior of degrading structural members. This is valuable for developing better design and safety codes.

The rest of the paper is organized as follows. Section 2 introduces the notation, mathematical preliminaries, and the relevant balance laws. Section 3 presents a mathematical model for degradation of materials due to moisture and temperature, which is valid even under finite deformations and large strains. The constitutive relations are obtained by appealing to the maximization of rate of dissipation hypothesis, which ensures that the constitutive model satisfies the second law of thermodynamics a priori. In Sect. 4, the proposed model is calibrated with an experimental data set. The coupled initial boundary value problem arising from the proposed degradation model is presented in Sect. 5. We also show the solutions of the proposed mathematical model are bounded and stable. In Sect. 6, solutions to several canonical problems are presented to illustrate the predictive capabilities of the proposed model and to highlight the effects of degradation on the structural behavior. Finally, conclusions are drawn in Sect. 7.

A list of the main symbols used in the paper is provided in the nomenclature.

2 Notation, preliminaries, and balance laws

Let us consider a body $\mathfrak{B}$. The body occupies a reference configuration $\Omega_0(\mathfrak{B}) \subset \mathbb{R}^{nd}$, where "$nd$" denotes the number of spatial dimensions. A point in the reference configuration is denoted by $\mathbf{p} \in \Omega_0(\mathfrak{B})$. We denote the time by $t \in [0, \mathcal{T}]$, where $\mathcal{T}$ is the length of the time interval of interest. Due to motion, the body occupies different spatial configurations with time. We denote the configuration occupied by the body at time t by $\Omega_t(\mathfrak{B}) \subset \mathbb{R}^{nd}$. A corresponding spatial point will be denoted by $\mathbf{x} \in \Omega_t(\mathfrak{B})$. The gradient and divergence operators with respect to $\mathbf{p}$ are, respectively, denoted by Grad[•] and Div[•]. Similarly, the gradient and divergence operators with respect to $\mathbf{x}$ are, respectively, denoted by grad[•] and div[•].

The motion of the body is mathematically described by the following invertible mapping:

$$\mathbf{x} = \boldsymbol{\varphi}(\mathbf{p}, t) \tag{2.1}$$

The displacement vector field can then be written as:

$$\mathbf{u} = \mathbf{x} - \mathbf{p} = \boldsymbol{\varphi}(\mathbf{p}, t) - \mathbf{p} \tag{2.2}$$

The velocity vector field is defined as:

$$\mathbf{v} = \dot{\mathbf{x}} := \frac{\partial \boldsymbol{\varphi}(\mathbf{p}, t)}{\partial t} \tag{2.3}$$

where a superposed dot indicates the material/total time derivative, which is the derivative with respect to time holding the reference coordinates fixed. The gradient of motion (which is also referred to as the deformation gradient) is defined as:

$$\mathbf{F} = \text{Grad}[\mathbf{x}] \equiv \frac{\partial \boldsymbol{\varphi}(\mathbf{p}, t)}{\partial \mathbf{p}} = \mathbf{I} + \text{Grad}[\mathbf{u}] \tag{2.4}$$

where $\mathbf{I}$ denotes the second-order identity tensor. The corresponding right Cauchy–Green tensor is denoted by:

$$\mathbf{C} = \mathbf{F}^{\mathrm{T}}\mathbf{F} \tag{2.5}$$

where $(\bullet)^{\mathrm{T}}$ denotes the transpose of a second-order tensor. The velocity gradient with respect to $\mathbf{x}$ and the symmetric part of the velocity gradient are, respectively, defined as follows:

$$\mathbf{L} := \text{grad}[\mathbf{v}] \equiv \dot{\mathbf{F}}\mathbf{F}^{-1} \tag{2.6}$$

$$\mathbf{D} := \frac{1}{2}\left(\mathbf{L} + \mathbf{L}^{\mathrm{T}}\right) \tag{2.7}$$

The Green-St. Venant strain tensor is defined as:

$$\mathbf{E} = \frac{1}{2}(\mathbf{C} - \mathbf{I}) = \frac{1}{2}\left(\text{Grad}[\mathbf{u}] + \text{Grad}[\mathbf{u}]^{\text{T}} + \text{Grad}[\mathbf{u}]^{\text{T}}\text{Grad}[\mathbf{u}]\right) \tag{2.8}$$

In those situations in which the following assumption holds:

$$\max_{\mathbf{p}\in\Omega_0(\mathfrak{B}),t\in[0,\mathcal{T}]} \sqrt{\|\boldsymbol{\varphi}(\mathbf{p},t) - \mathbf{p}\|^2 + \|\text{Grad}[\mathbf{u}]\|^2} \ll 1 \tag{2.9}$$

one is justified to employ the linearized strain tensor:

$$\mathbf{E}_l = \frac{1}{2}\left(\text{Grad}[\mathbf{u}] + \text{Grad}[\mathbf{u}]^{\text{T}}\right) \approx \frac{1}{2}\left(\text{grad}[\mathbf{u}] + \text{grad}[\mathbf{u}]^{\text{T}}\right) \tag{2.10}$$

where $\| \bullet \|$ denotes the Frobenius norm [5].

Since we will also be dealing with processes other than the mechanical deformation, we need to introduce quantities, which are in addition to the ones associated with the kinematics. We will denote the temperature by ϑ and the specific entropy by η. The mass fraction of the chemical species is denoted by c, and the corresponding chemical potential is denoted by $\varkappa$. The temperature, mass fraction of chemical species, entropy, and chemical potential are all scalar fields, while the displacement, velocity, and acceleration are vector fields. In some situations, it may be needed to explicitly indicate the functional dependence of these quantities. We employ a standard notation, which will be illustrated through the temperature field. The temperature in terms of reference coordinates and spatial coordinates will be denoted as follows:

$$\vartheta = \tilde{\vartheta}(\mathbf{p},t) = \hat{\vartheta}(\mathbf{x},t) \tag{2.11}$$

2.1 Balance laws

In our study, we take the entire degrading body to be the thermodynamic system. Moreover, we assume this thermodynamic system to be open. That is, heat and mass transfers can occur across the boundary of the system. We now document the balance laws that govern the evolution of the chosen system.

The *balance of mass for the solid* in the degrading body takes the following form:

$$\dot{\rho} + \rho\,\text{div}[\mathbf{v}] = 0 \tag{2.12}$$

where ρ is the density of the solid in the deformed configuration $\Omega_t(\mathfrak{B})$. The *balance of a chemical species*, which is being transported in the degrading body, can be mathematically written as:

$$\rho\dot{c} + \text{div}[\mathbf{h}] = h \tag{2.13}$$

where $\mathbf{h}$ is the mass transfer flux vector in the deformed configuration and h is the volumetric source of the chemical species in the deformed configuration. We assume that the chemical species cannot take partial stresses, which is a reasonable assumption in the degradation of materials due to small concentrations of moisture. One can handle large moisture contents by introducing partial stresses and using the theory of interacting continua (which is often referred to mixture theory) [12]. We do not address such issues, as our focus is degradation due to small concentrations of moisture or chemicals. The *balance of linear momentum for the solid* can be written as:

$$\rho\dot{\mathbf{v}} = \text{div}[\mathbf{T}] + \rho\mathbf{b} \tag{2.14}$$

where $\mathbf{b}$ is the specific body force and $\mathbf{T}$ is the Cauchy stress in the solid. Assuming that there is no internal couples, the *balance of angular momentum of the solid* reads:

$$\mathbf{T} = \mathbf{T}^{\text{T}} \tag{2.15}$$

Assuming that the balance of linear and angular momenta (i.e., Eqs. (2.14), (2.15)) holds, the *balance of energy of the system* (i.e., the first law of thermodynamics) can be written as:

$$\rho\frac{\text{d}}{\text{d}t}(A + \vartheta\eta) = \mathbf{T} \bullet \mathbf{D} - \text{div}[\varkappa\mathbf{h}] + \varkappa h - \text{div}[\mathbf{q}] + q \tag{2.16}$$

where A is the specific Helmholtz potential, $\mathbf{q}$ is the heat flux vector in the deformed configuration, and q is the volumetric heat source in the deformed configuration. In our study, we assume the Helmholtz potential A to depend on $\mathbf{F}$, c and ϑ. We also have the following relations for the chemical potential and the specific entropy:

$$\varkappa := +\frac{\partial A}{\partial c} \tag{2.17}$$

$$\eta := -\frac{\partial A}{\partial \vartheta} \tag{2.18}$$

Assuming the balance of chemical species to hold, we then have the following convenient form for the balance of energy:

$$\rho\left(\frac{\partial A}{\partial \mathbf{F}}\mathbf{F}^{\mathrm{T}} \bullet \mathbf{D} + \vartheta\dot{\eta}\right) = \mathbf{T} \bullet \mathbf{D} - \operatorname{div}[\mathbf{q}] - \operatorname{grad}[\varkappa] \bullet \mathbf{h} + q \tag{2.19}$$

The *reduced energy dissipation equation* (by assuming that all the aforementioned balance laws to hold) takes the following form:

$$\rho\left(\frac{\partial A}{\partial \mathbf{F}}\mathbf{F}^{\mathrm{T}} \bullet \mathbf{D}\right) = \mathbf{T} \bullet \mathbf{D} - \frac{1}{\vartheta}\operatorname{grad}[\vartheta] \bullet \mathbf{q} - \operatorname{grad}[\varkappa] \bullet \mathbf{h} - \rho\zeta, \quad \zeta \geq 0 \tag{2.20}$$

where ζ is the specific rate of dissipation functional, which is non-negative. The above equation is a stronger version than the second law of thermodynamics, which is an integral inequality. The second law of thermodynamics does *not* assert that the rate of entropy production be non-decreasing at *each and every point* in the system/body.

2.2 The maximization of rate of dissipation

Among the various methodologies to derive constitutive relations (e.g., see [48]), the maximization of rate of dissipation hypothesis put forth by Ziegler [83] is an attractive procedure. Herein, we extend this procedure to the open thermodynamic system that is under consideration. We obtain the constitutive relations using the maximization of rate of dissipation hypothesis, which needs the prescription of two functionals—the Helmholtz potential and the dissipation functional. We assume the functional dependence of the Helmholtz potential and the dissipation functional to be $\hat{A}(\mathbf{F}, c, \vartheta)$ and $\hat{\zeta}(\mathbf{D}, \operatorname{grad}[\vartheta], \operatorname{grad}[\varkappa]; \mathbf{F}, \vartheta, c)$.

The mathematical statement of the maximization of rate of dissipation can be written as follows:

$$\underset{\mathbf{D},\operatorname{grad}[\vartheta],\operatorname{grad}[\varkappa]}{\text{maximize}} \quad \rho\zeta = \rho\hat{\zeta}(\mathbf{D}, \operatorname{grad}[\vartheta], \operatorname{grad}[\varkappa]; \mathbf{F}, \vartheta, c) \tag{2.21a}$$

$$\text{subject to} \quad \rho\left(\frac{\partial A}{\partial \mathbf{F}}\mathbf{F}^{\mathrm{T}} \bullet \mathbf{D}\right) = \mathbf{T} \bullet \mathbf{D} - \frac{1}{\vartheta}\operatorname{grad}[\vartheta] \bullet \mathbf{q} - \operatorname{grad}[\varkappa] \bullet \mathbf{h} - \rho\zeta \tag{2.21b}$$

Note that $\rho\zeta$ is maximized with respect to arguments to the left of ";." Using the method of Lagrange multipliers, the above-constrained optimization problem is equivalent to the following unconstrained optimization problem:

$$\begin{aligned}\underset{\mathbf{D},\operatorname{grad}[\vartheta],\operatorname{grad}[\varkappa],\Lambda_t}{\text{extremize}} \quad & \rho\hat{\zeta}(\mathbf{D}, \operatorname{grad}[\vartheta], \operatorname{grad}[\varkappa]; \mathbf{F}, \vartheta, c) \\ & + \Lambda_t\left(\rho\left(\frac{\partial A}{\partial \mathbf{F}}\mathbf{F}^{\mathrm{T}} \bullet \mathbf{D}\right) - \mathbf{T} \bullet \mathbf{D} + \frac{1}{\vartheta}\operatorname{grad}[\vartheta] \bullet \mathbf{q} + \operatorname{grad}[\varkappa] \bullet \mathbf{h} + \rho\zeta\right)\end{aligned} \tag{2.22}$$

where Λ_t is the Lagrange multiplier enforcing the constraint (2.21b). The first-order optimal conditions give rise to the following relations:

$$\mathbf{T} = \rho\frac{\partial A}{\partial \mathbf{F}}\mathbf{F}^{\mathrm{T}} + \left(\frac{1+\Lambda_t}{\Lambda_t}\right)\rho\frac{\partial \zeta}{\partial \mathbf{D}} \tag{2.23a}$$

$$\frac{1}{\vartheta}\mathbf{q} = -\left(\frac{1+\Lambda_t}{\Lambda_t}\right)\rho\frac{\partial \zeta}{\partial \operatorname{grad}[\vartheta]} \tag{2.23b}$$

$$\mathbf{h} = -\left(\frac{1+\Lambda_t}{\Lambda_t}\right)\rho\frac{\partial\zeta}{\partial \text{grad}[\varkappa]} \tag{2.23c}$$

$$\rho\left(\frac{\partial A}{\partial \mathbf{F}}\mathbf{F}^{\mathrm{T}} \bullet \mathbf{D}\right) - \mathbf{T} \bullet \mathbf{D} + \frac{1}{\vartheta}\text{grad}[\vartheta] \bullet \mathbf{q} + \text{grad}[\varkappa] \bullet \mathbf{h} + \rho\zeta = 0 \tag{2.23d}$$

The above equations can be obtained by taking (Gâteaux) variation of the objective function in Eq. (2.22) with respect to $\mathbf{D}$, grad$[\vartheta]$, grad$[\varkappa]$, and Λ_t, respectively. By straightforward manipulations on Eqs. (2.23a)–(2.23d), the Lagrange multiplier Λ_t can be explicitly calculated as follows:

$$\Lambda_t = \left[\frac{\zeta}{\frac{\partial\zeta}{\partial\mathbf{D}} \bullet \mathbf{D} + \frac{\partial\zeta}{\partial \text{grad}[\vartheta]} \bullet \text{grad}[\vartheta] + \frac{\partial\zeta}{\partial \text{grad}[\varkappa]} \bullet \text{grad}[\varkappa]} - 1\right]^{-1} \tag{2.24}$$

If the rate of dissipation functional ζ is a homogeneous functional of order two with respect to $\mathbf{D}$, grad$[\vartheta]$, and grad$[\varkappa]$, we then have

$$\frac{\partial\zeta}{\partial\mathbf{D}} \bullet \mathbf{D} + \frac{\partial\zeta}{\partial \text{grad}[\vartheta]} \bullet \text{grad}[\vartheta] + \frac{\partial\zeta}{\partial \text{grad}[\varkappa]} \bullet \text{grad}[\varkappa] = 2\zeta \tag{2.25}$$

which further implies that $\Lambda_t = -2$. The constitutive relations under $\Lambda_t = -2$ will simplify to:

$$\mathbf{T} = \rho\frac{\partial A}{\partial \mathbf{F}}\mathbf{F}^{\mathrm{T}} + \frac{1}{2}\rho\frac{\partial\zeta}{\partial\mathbf{D}} \tag{2.26a}$$

$$\mathbf{q} = -\frac{\vartheta}{2}\rho\frac{\partial\zeta}{\partial \text{grad}[\vartheta]} \tag{2.26b}$$

$$\mathbf{h} = -\frac{1}{2}\rho\frac{\partial\zeta}{\partial \text{grad}[\varkappa]} \tag{2.26c}$$

It should be emphasized that the dissipation functional need not be a homogeneous functional of order two in terms of $\mathbf{F}$, c and ϑ. The maximization of the rate of dissipation hypothesis certainly does not require such an assumption. However, we will make such an assumption in Sect. 3, as it is convenient and the resulting constitutive relations can still model the desired degradation mechanisms.

2.3 Governing equations in the reference configuration

Since we are also interested in developing a computational framework and obtaining numerical solutions, it will be convenient to write the balance laws in the reference configuration. To this end, we introduce:

$$J \equiv \det[\mathbf{F}] \tag{2.27}$$

where det$[\bullet]$ denotes the determinant. The balance of mass in the reference configuration can be written as:

$$\rho_0 = J\rho \tag{2.28}$$

where ρ_0 is the density of the undeformed solid. The balance of chemical species in the reference configuration can be rewritten as:

$$\rho_0\dot{c} + \text{Div}[\mathbf{h}_0] = h_0 \tag{2.29}$$

where $\mathbf{h}_0 = J\mathbf{F}^{-1}\mathbf{h}$ is the diffusive flux vector in the reference configuration and $h_0 = Jh$ is the volumetric source in the reference configuration. The balance of linear momentum in the reference configuration takes the following form:

$$\rho_0\dot{\mathbf{v}} = \text{Div}[\mathbf{P}] + \rho_0\mathbf{b} \tag{2.30}$$

where $\mathbf{P} = J\mathbf{T}\mathbf{F}^{-\mathrm{T}}$ is the first Piola–Kirchhoff stress. The balance of angular momentum in the reference configuration takes the following form:

$$\mathbf{P}\mathbf{F}^{\mathrm{T}} = \mathbf{F}\mathbf{P}^{\mathrm{T}} \tag{2.31}$$

In the reference configuration, the balance of energy can be written as:

$$\rho_0 \left(\frac{\partial A}{\partial \mathbf{F}} \bullet \dot{\mathbf{F}} + \vartheta \dot{\eta} \right) = \mathbf{P} \bullet \dot{\mathbf{F}} - \text{Div}[\mathbf{q}_0] - \text{Grad}[\varkappa] \bullet \mathbf{h}_0 + q_0 \tag{2.32}$$

where $\mathbf{q}_0 = J\mathbf{F}^{-1}\mathbf{q}$ is the heat flux vector in the reference configuration and $q_0 = Jq$ is the volumetric heat source in the reference configuration. The reduced energy dissipation equation in the reference configuration can be rewritten as:

$$\rho_0 \left(\frac{\partial A}{\partial \mathbf{F}} \bullet \dot{\mathbf{F}} \right) = \mathbf{P} \bullet \dot{\mathbf{F}} - \frac{1}{\vartheta} \text{Grad}[\vartheta] \bullet \mathbf{q}_0 - \text{Grad}[\varkappa] \bullet \mathbf{h}_0 - \rho_0 \zeta_0 \tag{2.33}$$

where $\zeta_0 = \zeta$ is the non-negative rate of dissipation functional in the reference configuration.

2.3.1 Maximization of rate of dissipation in the reference configuration

The corresponding mathematical statement can be written as follows:

$$\underset{\dot{\mathbf{F}}, \text{Grad}[\vartheta], \text{Grad}[\varkappa]}{\text{maximize}} \quad \rho_0 \zeta_0 = \rho_0 \tilde{\zeta} (\dot{\mathbf{F}}, \text{Grad}[\vartheta], \text{Grad}[\varkappa]; \mathbf{F}, \vartheta, c) \tag{2.34a}$$

$$\text{subject to} \quad \rho_0 \left(\frac{\partial A}{\partial \mathbf{F}} \bullet \dot{\mathbf{F}} \right) = \mathbf{P} \bullet \dot{\mathbf{F}} - \frac{1}{\vartheta} \text{Grad}[\vartheta] \bullet \mathbf{q}_0 - \text{Grad}[\varkappa] \bullet \mathbf{h}_0 - \rho_0 \zeta_0 \tag{2.34b}$$

Using the method of Lagrange multipliers, one can obtain the following equivalent unconstrained optimization problem:

$$\begin{aligned} \underset{\dot{\mathbf{F}}, \text{Grad}[\vartheta], \text{Grad}[\varkappa], \Lambda_0}{\text{extremize}} \quad & \rho_0 \tilde{\zeta} (\dot{\mathbf{F}}, \text{Grad}[\vartheta], \text{Grad}[\varkappa]; \mathbf{F}, \vartheta, c) \\ & + \Lambda_0 \left(\rho_0 \left(\frac{\partial A}{\partial \mathbf{F}} \bullet \dot{\mathbf{F}} \right) - \mathbf{P} \bullet \dot{\mathbf{F}} + \frac{1}{\vartheta} \text{Grad}[\vartheta] \bullet \mathbf{q}_0 + \text{Grad}[\varkappa] \bullet \mathbf{h}_0 + \rho_0 \zeta_0 \right) \end{aligned} \tag{2.35}$$

where Λ_0 is the Lagrange multiplier enforcing the constraint given by Eq. (2.34b). The first-order optimality conditions give rise to the following constitutive relations:

$$\mathbf{P} = \rho_0 \frac{\partial A}{\partial \mathbf{F}} + \left(\frac{1 + \Lambda_0}{\Lambda_0} \right) \rho_0 \frac{\partial \zeta_0}{\partial \dot{\mathbf{F}}} \tag{2.36a}$$

$$\frac{1}{\vartheta} \mathbf{q}_0 = - \left(\frac{1 + \Lambda_0}{\Lambda_0} \right) \rho_0 \frac{\partial \zeta_0}{\partial \text{Grad}[\vartheta]} \tag{2.36b}$$

$$\mathbf{h}_0 = - \left(\frac{1 + \Lambda_0}{\Lambda_0} \right) \rho_0 \frac{\partial \zeta_0}{\partial \text{Grad}[\varkappa]} \tag{2.36c}$$

$$\rho_0 \left(\frac{\partial A}{\partial \mathbf{F}} \bullet \dot{\mathbf{F}} \right) - \mathbf{P} \bullet \dot{\mathbf{F}} + \frac{1}{\vartheta} \text{Grad}[\vartheta] \bullet \mathbf{q}_0 + \text{Grad}[\varkappa] \bullet \mathbf{h}_0 + \rho_0 \zeta_0 = 0 \tag{2.36d}$$

Similar to the derivation presented earlier in the context of current configuration, the Lagrange multiplier Λ_0 can be explicitly calculated as follows:

$$\Lambda_0 = \left[\frac{\zeta_0}{\frac{\partial \zeta_0}{\partial \dot{\mathbf{F}}} \bullet \dot{\mathbf{F}} + \frac{\partial \zeta_0}{\partial \text{Grad}[\vartheta]} \bullet \text{Grad}[\vartheta] + \frac{\partial \zeta_0}{\partial \text{Grad}[\varkappa]} \bullet \text{Grad}[\varkappa]} - 1 \right]^{-1} \tag{2.37}$$

If the rate of dissipation functional in the reference configuration ζ_0 is a homogeneous functional of order two, we have

$$\frac{\partial \zeta_0}{\partial \dot{\mathbf{F}}} \bullet \dot{\mathbf{F}} + \frac{\partial \zeta_0}{\partial \text{Grad}[\vartheta]} \bullet \text{Grad}[\vartheta] + \frac{\partial \zeta_0}{\partial \text{Grad}[\varkappa]} \bullet \text{Grad}[\varkappa] = 2\zeta_0 \tag{2.38}$$

which further implies that $\Lambda_0 = -2$. The constitutive relations under $\Lambda_0 = -2$ take the following form:

$$\mathbf{P} = \rho_0 \frac{\partial A}{\partial \mathbf{F}} + \frac{1}{2} \rho_0 \frac{\partial \zeta_0}{\partial \dot{\mathbf{F}}} \tag{2.39a}$$

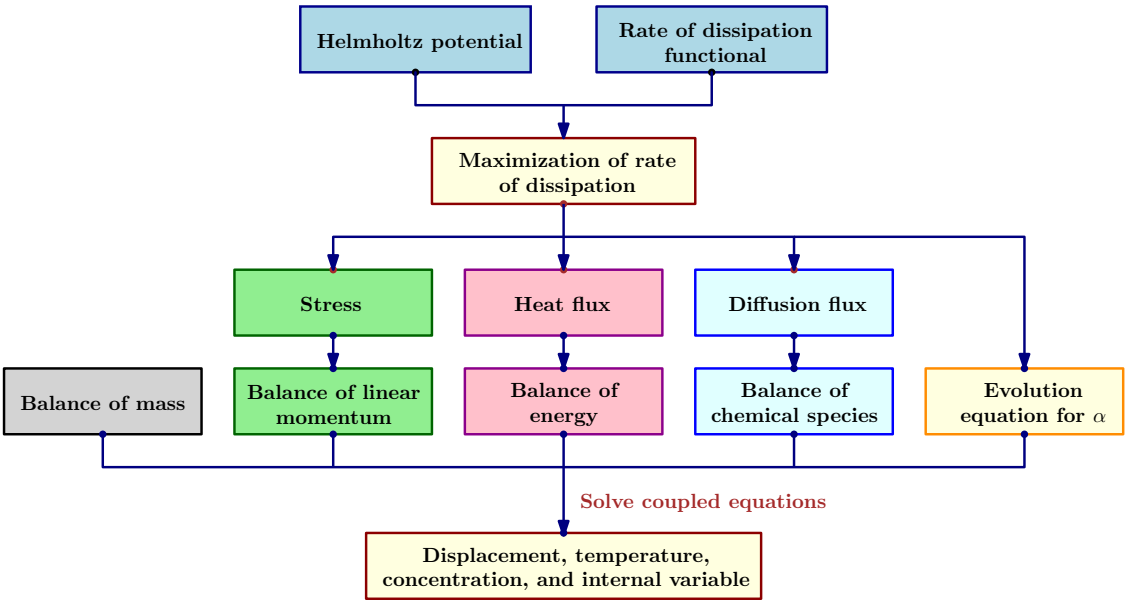

Fig. 1 Overarching idea of the proposed degradation framework: This flowchart shows the overarching idea behind the proposed framework. We appeal to the maximization of rate of dissipation hypothesis to obtain constitutive relations for the stress, heat flux, diffusion flux, and evolution equation for an internal variable. By solving the resulting coupled equations (i.e, balance laws, constitutive relations, and boundary and initial conditions), one can obtain the displacement, temperature, concentration, and internal variable fields

$$\mathbf{q}_0 = -\frac{\vartheta}{2}\rho_0 \frac{\partial \zeta_0}{\partial \text{Grad}[\vartheta]} \tag{2.39b}$$

$$\mathbf{h}_0 = -\frac{1}{2}\rho_0 \frac{\partial \zeta_0}{\partial \text{Grad}[\varkappa]} \tag{2.39c}$$

The overarching idea behind the proposed chemo–thermo–mechano degradation model is shown in Fig. 1. In the next section, we will develop the proposed constitutive model by appealing to the maximization of rate of dissipation.

3 A general constitutive model for chemo–thermo–mechano degradation

Under the maximization of rate of dissipation hypothesis, the constitutive relations can be obtained by prescribing two functionals—the Helmholtz potential and the dissipation functional. Philosophically, the Helmholtz potential quantifies the way in which the material stores energy, whereas the dissipation functional quantifies the way in which the material dissipates energy. For our proposed chemo–thermo–mechano degradation model, we prescribe the following functional forms for the specific Helmholtz potential and the rate of dissipation functional:

$$\begin{aligned} A = \hat{A}(\mathbf{F}, c, \vartheta) = \frac{1}{\rho_0}\psi - \frac{1}{2}\frac{c_p}{\vartheta_{\text{ref}}}\{\vartheta - \vartheta_{\text{ref}}\}^2 - \frac{1}{\rho_0}\{\vartheta - \vartheta_{\text{ref}}\}\,\mathbf{M}_{\vartheta\mathbf{E}} \bullet \mathbf{E} \\ + d_{\vartheta c}\{\vartheta - \vartheta_{\text{ref}}\}\{c - c_{\text{ref}}\} - \frac{1}{\rho_0}\{c - c_{\text{ref}}\}\,\mathbf{M}_{c\mathbf{E}} \bullet \mathbf{E} + \frac{R_s\vartheta_{\text{ref}}}{2}\{c - c_{\text{ref}}\}^2 \end{aligned} \tag{3.1}$$

$$\begin{aligned} \zeta = \hat{\zeta}(\mathbf{D}, \text{grad}[\vartheta], \text{grad}[\varkappa]; \mathbf{F}, \vartheta, c) = \frac{c_p}{\vartheta}\text{grad}[\vartheta] \bullet \mathbf{D}_{\vartheta\vartheta}\text{grad}[\vartheta] + \frac{1}{\vartheta}\text{grad}[\vartheta] \bullet \mathbf{D}_{\vartheta\varkappa}\text{grad}[\varkappa] \\ + \frac{1}{\vartheta}\text{grad}[\varkappa] \bullet \mathbf{D}_{\varkappa\vartheta}\text{grad}[\vartheta] + \frac{1}{R_s\vartheta_{\text{ref}}}\text{grad}[\varkappa] \bullet \mathbf{D}_{\varkappa\varkappa}\text{grad}[\varkappa] \end{aligned} \tag{3.2}$$

where $R_s = R/M$. R_s and R denote the specific vapor constant and the universal vapor constant, respectively, M is the molecular mass of chemical species. ϑ_{ref} and c_{ref} are the specified reference temperature and reference

mass concentration, which depend on the underlying boundary value problem. We denote c_p as the coefficient of heat capacity, $d_{\vartheta c}$ as the thermo-chemo coupled parameter [68], $\mathbf{M}_{\vartheta\mathbf{E}}$ as the anisotropic coefficient of thermal expansion (which is assumed to be independent of temperature, concentration, and strain), and $\mathbf{M}_{c\mathbf{E}}$ as the anisotropic coefficient of chemical expansion due to concentration (which is also assumed to be independent of temperature, concentration, and strain). Both $\mathbf{M}_{\vartheta\mathbf{E}}$ and $\mathbf{M}_{c\mathbf{E}}$ are assumed to be symmetric. $\mathbf{D}_{\vartheta\vartheta}$ is the anisotropic thermal conductivity tensor and $\mathbf{D}_{\varkappa\varkappa}$ is the anisotropic diffusivity tensor. $\mathbf{D}_{\vartheta\varkappa}$ corresponds to the anisotropic Soret effect tensor, which characterizes the transport of chemical species caused by temperature gradient. Similarly, $\mathbf{D}_{\varkappa\vartheta}$ is the Dufour effect tensor, which represents the heat flow caused by a concentration gradient.

Remark 3.1 In chemo–thermo-elasticity and in modeling degradation of materials due to transport and reaction of chemical species, coefficient of chemical expansion $\mathbf{M}_{c\mathbf{E}}$ and thermo-chemo coupling parameter $d_{\vartheta c}$ play a vital role (see [68, Chapter-5] and references therein). Induced strains due to chemical expansivity will be significant in harsh environmental conditions and cannot be neglected [68]. Considerable inquest has been made in the literature to experimentally measure $\mathbf{M}_{c\mathbf{E}}$ in ceramics [2,9,51], laminated and polymer composites [10,14,68], elastomers and biological materials [32,43,54], and concrete structures [15,72,73]. However, adequate progress has not been made yet to develop constitutive models and computational frameworks for such chemo–thermo-elastic materials or materials undergoing chemical-induced degradation. Herein, we shall take a step forward to address this issue.

Remark 3.2 It should be noted that in the absence of electrical and magnetic fields, all of the above tensors are symmetric [12,19,36]. Moreover, from the Onsager reciprocal relations (which was put forth by Onsager in 1930s [57,58]) we have the following relationship between the Soret effect tensor and the Dufour effect tensor.

$$\mathbf{D}_{\vartheta\varkappa} = \mathbf{D}_{\varkappa\vartheta} \tag{3.3}$$

Additionally, physics demands that the tensors $\mathbf{D}_{\vartheta\vartheta}$ and $\mathbf{D}_{\varkappa\varkappa}$ are positive definite.

Remark 3.3 Note that the specific Helmholtz potential and correspondingly the dissipation functional for diffusion can also be modeled using the following expressions:

$$A_c = R_s\vartheta_{\text{ref}}c\{\ln[c] - 1\} \tag{3.4}$$

$$\zeta_c = \frac{c}{R_s\vartheta_{\text{ref}}}\text{grad}[\varkappa] \bullet \mathbf{D}_{\varkappa\varkappa}\text{grad}[\varkappa] \tag{3.5}$$

Both Eqs. (3.1)–(3.2) and (3.4)–(3.5) result in similar partial differential equation structure for modeling Fickian diffusion.

Under the proposed model, the specific entropy and chemical potential take the following form:

$$\eta = -\frac{\partial A}{\partial\vartheta} = -\frac{1}{\rho_0}\frac{\partial\psi}{\partial\vartheta} + \frac{c_p}{\vartheta_{\text{ref}}}\{\vartheta - \vartheta_{\text{ref}}\} + \frac{1}{\rho_0}\mathbf{M}_{\vartheta\mathbf{E}} \bullet \mathbf{E} - d_{\vartheta c}\{c - c_{\text{ref}}\} \tag{3.6}$$

$$\varkappa = \frac{\partial A}{\partial c} = \frac{1}{\rho_0}\frac{\partial\psi}{\partial c} + R_s\vartheta_{\text{ref}}\{c - c_{\text{ref}}\} - \frac{1}{\rho_0}\mathbf{M}_{c\mathbf{E}} \bullet \mathbf{E} + d_{\vartheta c}\{\vartheta - \vartheta_{\text{ref}}\} \tag{3.7}$$

From Eqs. (2.26a)–(2.26c), we have the constitutive relations in deformed configuration as:

$$\mathbf{T} = \rho\frac{\partial A}{\partial\mathbf{F}}\mathbf{F}^{\text{T}} = \frac{1}{J}\frac{\partial\psi}{\partial\mathbf{F}}\mathbf{F}^{\text{T}} - \frac{1}{J}\{\vartheta - \vartheta_{\text{ref}}\}\mathbf{F}\mathbf{M}_{\vartheta\mathbf{E}}\mathbf{F}^{\text{T}} - \frac{1}{J}\{c - c_{\text{ref}}\}\mathbf{F}\mathbf{M}_{c\mathbf{E}}\mathbf{F}^{\text{T}} \tag{3.8a}$$

$$\mathbf{q} = -\frac{\vartheta}{2}\rho\frac{\partial\hat{\zeta}}{\partial\text{grad}[\vartheta]} = -\rho c_p\mathbf{D}_{\vartheta\vartheta}\text{grad}[\vartheta] - \frac{\rho}{2}\mathbf{D}_{\vartheta\varkappa}\text{grad}[\varkappa] - \frac{\rho}{2}\mathbf{D}_{\varkappa\vartheta}\text{grad}[\varkappa] \tag{3.8b}$$

$$\mathbf{h} = -\frac{1}{2}\rho\frac{\partial\hat{\zeta}}{\partial\text{grad}[\varkappa]} = -\frac{\rho}{R_s\vartheta_{\text{ref}}}\mathbf{D}_{\varkappa\varkappa}\text{grad}[\varkappa] - \frac{\rho}{2\vartheta}\mathbf{D}_{\vartheta\varkappa}\text{grad}[\vartheta] - \frac{\rho}{2\vartheta}\mathbf{D}_{\varkappa\vartheta}\text{grad}[\vartheta] \tag{3.8c}$$

The rate of dissipation functional for the degradation model in the reference configuration is taken as follows:

$$\begin{aligned}\zeta &= \tilde{\zeta}(\dot{\mathbf{F}}, \mathrm{Grad}[\vartheta], \mathrm{Grad}[\varkappa]; \mathbf{F}, \vartheta, c)\\ &= \frac{c_p}{\vartheta}\mathrm{Grad}[\vartheta] \bullet \overline{\mathbf{D}}_{\vartheta\vartheta}\mathrm{Grad}[\vartheta] + \frac{1}{\vartheta}\mathrm{Grad}[\vartheta] \bullet \overline{\mathbf{D}}_{\vartheta\varkappa}\mathrm{Grad}[\varkappa]\\ &\quad + \frac{1}{\vartheta}\mathrm{Grad}[\varkappa] \bullet \overline{\mathbf{D}}_{\varkappa\vartheta}\mathrm{Grad}[\vartheta] + \frac{1}{R_s\vartheta_{\mathrm{ref}}}\mathrm{Grad}[\varkappa] \bullet \overline{\mathbf{D}}_{\varkappa\varkappa}\mathrm{Grad}[\varkappa]\end{aligned} \tag{3.9}$$

where $\overline{\mathbf{D}}_{\alpha\beta} = \mathbf{F}^{-1}\mathbf{D}_{\alpha\beta}\mathbf{F}^{-T}$, in which α and β represent ϑ or $\varkappa$. Correspondingly, the constitutive relations in the reference configuration take the following form:

$$\mathbf{P} = \rho_0\frac{\partial A}{\partial \mathbf{F}} = \frac{\partial \psi}{\partial \mathbf{F}} - \{\vartheta - \vartheta_{\mathrm{ref}}\}\,\mathbf{F}\mathbf{M}_{\vartheta\mathbf{E}} - \{c - c_{\mathrm{ref}}\}\,\mathbf{F}\mathbf{M}_{c\mathbf{E}} \tag{3.10a}$$

$$\mathbf{q}_0 = -\frac{\vartheta}{2}\rho_0\frac{\partial \tilde{\zeta}}{\partial \mathrm{Grad}[\vartheta]} = -\rho_0 c_p\overline{\mathbf{D}}_{\vartheta\vartheta}\mathrm{Grad}[\vartheta] - \frac{\rho_0}{2}\overline{\mathbf{D}}_{\vartheta\varkappa}\mathrm{Grad}[\varkappa] - \frac{\rho_0}{2}\overline{\mathbf{D}}_{\varkappa\vartheta}\mathrm{Grad}[\varkappa] \tag{3.10b}$$

$$\mathbf{h}_0 = -\frac{1}{2}\rho_0\frac{\partial \tilde{\zeta}}{\partial \mathrm{Grad}[\varkappa]} = -\frac{\rho_0}{R_s\vartheta_{\mathrm{ref}}}\overline{\mathbf{D}}_{\varkappa\varkappa}\mathrm{Grad}[\varkappa] - \frac{\rho_0}{2\vartheta}\overline{\mathbf{D}}_{\vartheta\varkappa}\mathrm{Grad}[\vartheta] - \frac{\rho_0}{2\vartheta}\overline{\mathbf{D}}_{\varkappa\vartheta}\mathrm{Grad}[\vartheta] \tag{3.10c}$$

3.1 Coupling terms for the degradation model

The following hyperelastic material models will be employed in this paper:

$$\psi = \frac{\lambda}{2}(\mathrm{tr}[\mathbf{E}])^2 + \mu\mathbf{E} \bullet \mathbf{E} \qquad \text{St. Venant-Kirchhoff model} \tag{3.11a}$$

$$\psi = \frac{\kappa}{2}(\ln[J])^2 + \mu\mathbf{E} \bullet \mathbf{E} \qquad \text{Modified St. Venant-Kirchhoff model} \tag{3.11b}$$

$$\psi = \mu\mathrm{tr}[\mathbf{E}] + \mu\ln[J] + \frac{\lambda}{2}(\ln[J])^2 \qquad \text{Neo-Hookean model} \tag{3.11c}$$

where ψ is the stored strain energy density functional, λ and μ are the Lamé parameters, and $\kappa = \lambda + \frac{2\mu}{3}$ is the bulk modulus. Recall that $J = \det[\mathbf{F}]$. The Lamé parameters in the degrading model are given by the following expressions:

$$\lambda(\mathbf{x}, c) = \lambda_0(\mathbf{x}) - \lambda_1(\mathbf{x})\frac{c}{c_{\mathrm{ref}}} - \lambda_2(\mathbf{x})\frac{\vartheta}{\vartheta_{\mathrm{ref}}} \tag{3.12a}$$

$$\mu(\mathbf{x}, c) = \mu_0(\mathbf{x}) - \mu_1(\mathbf{x})\frac{c}{c_{\mathrm{ref}}} - \mu_2(\mathbf{x})\frac{\vartheta}{\vartheta_{\mathrm{ref}}} \tag{3.12b}$$

where λ_0 and μ_0 are the Lamé parameters of the virgin material. λ_1 and μ_1 are the parameters that account for the effect of concentration of chemical species on degradation of solid. λ_2 and μ_2 are the parameters that account for the temperature effect on the degrading solid. It should be noted that λ_1, μ_1, λ_2, and μ_2 are all positive. Furthermore, these parameters are constrained such that the bulk modulus and shear modulus are strictly positive.

3.1.1 Deformation-dependent diffusivity

The effect of deformation on diffusivity is modeled as follows: When tensile and shear strains are predominant, we have the following constitutive model

$$\begin{aligned}\mathbf{D}_{\varkappa\varkappa} = \mathbf{D}_0 &+ (\mathbf{D}_T - \mathbf{D}_0)\frac{(\exp[\eta_T I_{\mathbf{E}}] - 1)}{(\exp[\eta_T E_{\mathrm{ref}T}] - 1)} + (\mathbf{D}_S - \mathbf{D}_0)\frac{(\exp[\eta_S II_{\mathbf{E}}] - 1)}{(\exp[\eta_S E_{\mathrm{ref}S}] - 1)}\\ &+ (\mathbf{D}_{MS} - \mathbf{D}_0)\frac{(\exp[\eta_{MS} III_{\mathbf{E}}] - 1)}{(\exp[\eta_{MS} E_{\mathrm{ref}MS}] - 1)}\end{aligned} \tag{3.13}$$

where $I_{\mathbf{E}}$, $II_{\mathbf{E}}$, and $III_{\mathbf{E}}$ are the first, second, and third invariants of the Green-St. Venant strain tensor, respectively. These are defined as follows:

$$I_{\mathbf{E}} := \mathrm{tr}[\mathbf{E}] \tag{3.14a}$$

$$II_{\mathbf{E}} := \sqrt{2\,\mathrm{dev}[\mathbf{E}] \bullet \mathrm{dev}[\mathbf{E}]} = \sqrt{\frac{2}{3}(3\mathrm{tr}[\mathbf{E}^2] - (\mathrm{tr}[\mathbf{E}])^2)} \tag{3.14b}$$

$$III_{\mathbf{E}} := \det\left[\frac{1}{II_{\mathbf{E}}}\mathrm{dev}[\mathbf{E}]\right] \tag{3.14c}$$

where $\mathrm{dev}[\mathbf{E}] := \mathbf{E} - \frac{1}{3}\mathrm{tr}[\mathbf{E}]\mathbf{I}$ is the deviatoric part of $\mathbf{E}$. These invariants are used to model the effect of dilation, magnitude of distortion, and mode of distortion on the diffusivity of the solid. η_T, η_S, and η_{MS} are non-negative parameters. $E_{\mathrm{ref}T}$, $E_{\mathrm{ref}S}$, and $E_{\mathrm{ref}MS}$ are reference measures of the tensile strain, shear strain, and mode of shear strain, respectively. $\mathbf{D}_0$, $\mathbf{D}_T$, $\mathbf{D}_S$, and $\mathbf{D}_{MS}$ are, respectively, the reference diffusivity tensors under no strain, tensile strain, and shear strain.

When compression and shear strains are predominant, deformation-dependent diffusivity is modeled as follows:

$$\begin{aligned}\mathbf{D}_{\varkappa\varkappa} = \mathbf{D}_0 &+ (\mathbf{D}_0 - \mathbf{D}_C)\,\frac{(\exp[\eta_T I_{\mathbf{E}}] - 1)}{(\exp[\eta_T E_{\mathrm{ref}T}] - 1)} + (\mathbf{D}_S - \mathbf{D}_0)\,\frac{(\exp[\eta_S II_{\mathbf{E}}] - 1)}{(\exp[\eta_S E_{\mathrm{ref}S}] - 1)} \\ &+ (\mathbf{D}_{MS} - \mathbf{D}_0)\,\frac{(\exp[\eta_{MS} III_{\mathbf{E}}] - 1)}{(\exp[\eta_{MS} E_{\mathrm{ref}MS}] - 1)}\end{aligned} \tag{3.15}$$

where η_C is a non-negative parameter, $E_{\mathrm{ref}C}$ is a reference measure of the compression strain, and $\mathbf{D}_C$ is the reference diffusivity tensor under compressive strain.

Remark 3.4 Note that deformation-dependent diffusivity given by Eqs. (3.13) and (3.15) can be constructed using a different set of invariants of a given strain tensor. These invariants can be either principal or Hencky type [20,46,62] based on the nature of material and associated experimental data. The proposed framework can accommodate such models with minor modifications.

In case of transversely isotropic materials with fibers running along the direction $\mathbf{M}_{tf}$, the following invariants are needed to model deformation-dependent diffusivity in addition to the invariant set given by Eqs. (3.14a)–(3.14c)

$$IV_{\mathbf{E}} := \mathbf{M}_{tf} \bullet \mathbf{E}\mathbf{M}_{tf} \tag{3.16a}$$

$$V_{\mathbf{E}} := \mathbf{M}_{tf} \bullet \mathbf{E}^2\mathbf{M}_{tf} \tag{3.16b}$$

For more details on selection of invariants for transversely isotropic or orthotropic materials, see [35,46,56].

3.1.2 Deformation-dependent thermal conductivity

The effect of deformation of the solid on thermal conductivity is modeled as follows [7]:

$$\mathbf{D}_{\vartheta\vartheta} = \mathbf{K}_{0\vartheta}(1 + I_{\mathbf{E}})^{-\delta} \tag{3.17}$$

where δ is a non-negative parameter. $\mathbf{K}_{0\vartheta}$ is the reference conductivity tensor under no strain. Based on molecular dynamics simulations, Bhowmick and Shenoy [7] suggested δ to be 9.59 and $\mathbf{K}_{0\vartheta} = 4.61\vartheta^{-1.45}$ (for certain brittle-type materials). For various other ductile or brittle-type materials, these parameters can be determined by experiments or can be constructed using Lennard–Jones potential in molecular dynamics.

Remark 3.5 Due to the lack of experimental data, we assume that Dufour and Soret tensors do not depend on the deformation of solid. However, it should be noted that the proposed thermodynamic and computational framework can accommodate deformation-dependent Dufour and Soret tensors with minor modifications (whenever such an experimental evidence is available).

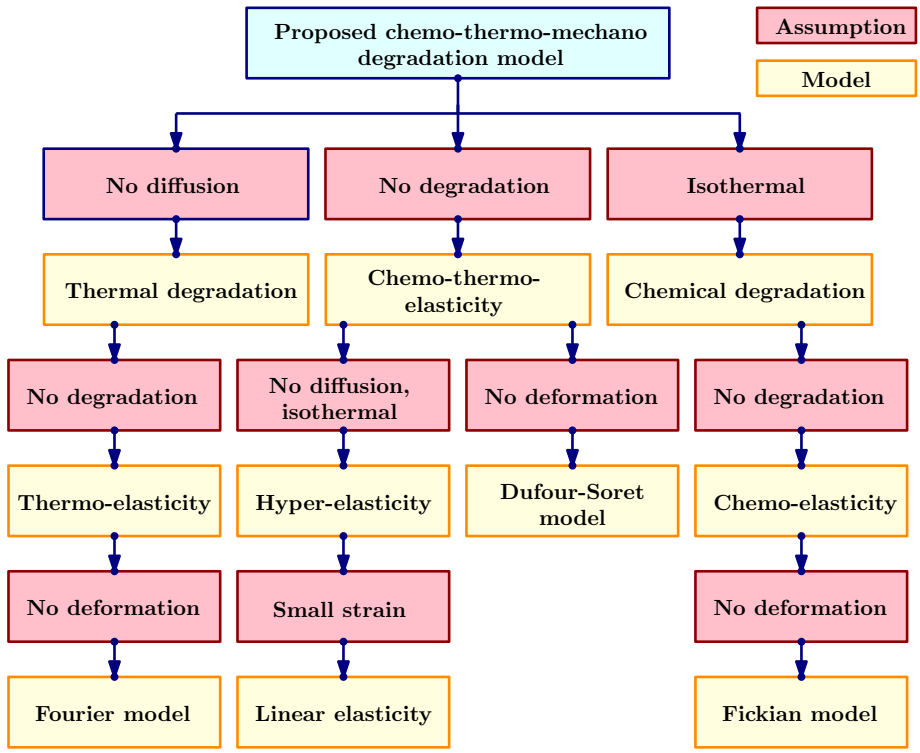

Fig. 2 Special cases of the proposed chemo–thermo–mechano degradation model: Many existing degrading and non-degrading constitutive models are special cases of the proposed hierarchical model, with appropriate assumptions

3.2 Special cases of the general degradation model and their thermodynamic status

The following popular non-degradation constitutive models can be shown as special cases of the proposed degradation model, as shown in Fig. 2, when the material parameters are assumed to be independent of concentration, temperature, and deformation of the solid. That is, the Lamé parameters and $\mathbf{D}_{\alpha\beta}$ (α and β represent either ϑ or $\varkappa$) are independent of c, ϑ, and $\mathbf{E}$.

1. `Fourier and Fickian models:` The standard heat conduction constitutive model is obtained by assuming the solid to be rigid and mass concentration of diffusing chemical species to be equal to zero. Similarly, to recover the standard Fickian model we assume the solid to be rigid and temperature of the homogenized body to be constant.
2. `Dufour-Soret model:` This model is obtained by assuming the solid to be rigid. Furthermore, the thermo-chemo coupling parameter $d_{\vartheta c}$ is neglected.
3. `Linearized elasticity and hyperelasticity:` To obtain hyperelastic constitutive models, we assume isothermal conditions and mass concentration of diffusing chemical species to be equal to zero. The linearized elasticity model can be recovered from any given hyperelastic model by assuming that the small-strain assumption given by Eq. (2.9) holds.
4. `Thermo-elasticity:` The standard thermo-elasticity model can be recovered by assuming mass concentration of diffusing chemical species to be equal to zero. The material parameters are assumed to be independent of temperature and deformation.
5. `Chemoelasticity:` Similarly, the standard chemoelasticity model can be recovered by assuming isothermal conditions. The material parameters are assumed to be independent of concentration and deformation.
6. `Chemo-Thermo-elasticity:` Herein, we assume that the material parameters are independent of concentration, temperature, and deformation. In addition, thermo-chemo coupling parameter $d_{\vartheta c}$, Dufour tensor, and Soret tensor are neglected.

One can also derive specialized (thermo-mechano and chemo-mechano) degradation models:

1. `Thermo-mechano degradation model:` This model is obtained from the thermo-elasticity model by relaxing the assumption that material parameters are independent of temperature and deformation.

2. `Chemo-mechano degradation model:` Similar to thermo-mechano degradation model, this degradation model is obtained from the chemoelasticity model by relaxing the assumption that material parameters are independent of concentration and deformation.

3.2.1 Status of the degradation model in [52]

The small-strain chemo-mechano degradation model proposed in [52] is a special case of the proposed chemo–thermo–mechano degradation and can be obtained under a plethora of assumptions. These assumptions include steady-state response, small strains, and isothermal conditions with negative volumetric heat source in the entire degrading body. One also needs to neglect chemo–thermo, chemo–mechano, and thermo–mechano couplings. Moreover, the functional forms of the specific Helmholtz potential and rate of dissipation functional need to be:

$$A = \frac{1}{\rho}\psi + \frac{R_s\vartheta_{\text{ref}}}{2}\{c - c_{\text{ref}}\}^2 \tag{3.18}$$

$$\zeta = \frac{1}{R_s\vartheta_{\text{ref}}}\text{grad}[\varkappa] \bullet \mathbf{D}_{\varkappa\varkappa}\text{grad}[\varkappa] \tag{3.19}$$

where the stored strain energy density functional is given by:

$$\psi = \hat{\psi}(\mathbf{E}_l, c) = \frac{\lambda(c)}{2}(\text{tr}[\mathbf{E}_l])^2 + \mu(c)\mathbf{E}_l \bullet \mathbf{E}_l \tag{3.20}$$

Under the small-strain assumption given by Eq. (2.9), the Cauchy stress, chemical potential, and mass transfer flux vector can be written as:

$$\mathbf{T} = \rho\frac{\partial A}{\partial \mathbf{E}_l} = \lambda(c)\text{tr}[\mathbf{E}_l]\mathbf{I} + 2\mu(c)\mathbf{E}_l \tag{3.21}$$

$$\varkappa = \frac{\partial A}{\partial c} = R_s\vartheta_{\text{ref}}\{c - c_{\text{ref}}\} \tag{3.22}$$

$$\mathbf{h} = -\frac{1}{2}\rho\frac{\partial\hat{\zeta}}{\partial\text{grad}[\varkappa]} = -\frac{\rho}{R_s\vartheta_{\text{ref}}}\mathbf{D}_{\varkappa\varkappa}\text{grad}[\varkappa] \tag{3.23}$$

The balance of chemical species and the balance of linear momentum for the solid are given by Eqs. (2.13) and (2.14). Under the isothermal condition, the balance of energy simplifies to the following expression:

$$q = -\frac{\rho}{R_s\vartheta_{\text{ref}}}\text{grad}[\varkappa] \bullet \mathbf{D}_{\varkappa\varkappa}\text{grad}[\varkappa] \tag{3.24}$$

which means that q needs to be non-positive in order to maintain the isothermal condition. The deformation-dependent diffusivity $\mathbf{D}_{\varkappa\varkappa}$ is based on the small-strain assumption, which is obtained by linearizing the Eqs. (3.13) and (3.15). Note that this model is developed based on the experimental evidence that the relative diffusion rate varies exponentially with respect to the trace of strain [49,50]. In this paper, we have taken a step further to calibrate these materials parameters according to the experimental data for finite strains based on the model given by Eqs. (3.13) and (3.15).

4 Calibration with experimental data

In this section, we will calibrate the proposed model for the diffusivity using the experimental data set reported in [49,50]. These experiments were conducted on spherical shells made of glass, which is a brittle material. These papers report the variation of diffusivity under various deformation modes: tension, compression, and shear. The calibration study presented below, which also includes a statistical analysis of the fit, will be valuable in two ways. *First*, it demonstrates the predictive capabilities of the proposed constitutive model and provides confidence in the model to be able to apply to other brittle materials like ceramics and even to quasi-brittle materials like concrete with appropriate modifications. *Second*, it provides order-of-magnitude estimates for various parameters in the diffusivity model for realistic materials. This will guide in the selection of values for these parameters in the subsequent numerical studies.

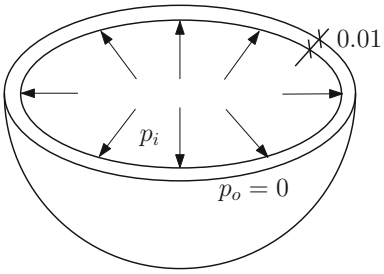

Fig. 3 Calibration with experimental data: A pictorial description of the degrading shell used for calibrating the proposed model with the experimental data. The inner pressure varies in the range of 0 to 100 psi. Experiments measure the change in diffusivity as well as the strain of the thin spherical shell. The obtained data can be used to calibrate the proposed model

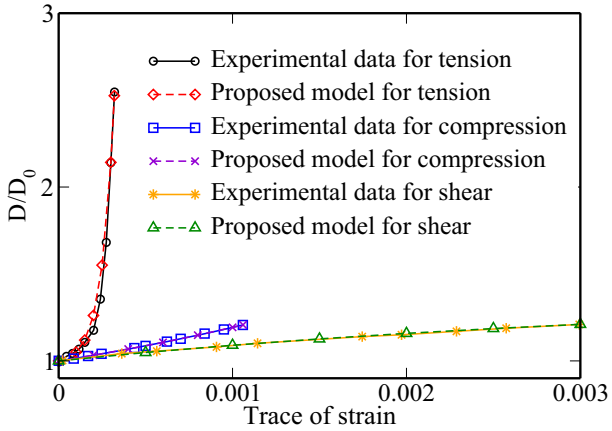

Fig. 4 Calibration with experimental data: This figure compares the experimental data reported in [49,50] with the proposed constitutive model. The sample size is taken to be three. The strain invariants are given by Eqs. (3.14a)–(3.14b). A good agreement has been observed between the experimental data and the proposed constitutive model for the diffusivity under tensile, compressive, and shear strains

Figure 3 provides the geometry and the loading on a spherical shell. The inner and outer radii are, respectively, $r_i = 0.99$ and $r_o = 1.0$. The boundary conditions for the deformation subproblem are that the pressure within the sphere is varied from $p_i = 0$ to $p_i = 0.68947$ MPa (100 psi) and the external surface is traction free. The diffusion can be assumed to be isotropic; therefore, the diffusivity tensor is simplified to a scalar. In this scenario, it can be assumed that the tensile strain is predominant. Hence, the shear-related terms in Eq. (3.13) can be ignored and then it can be simplified as follows:

$$D = D_0 + (D_T - D_0)\,\frac{(\exp[\eta_T I_{\mathbf{E}}] - 1)}{(\exp[\eta_T E_{\mathrm{ref}_T}] - 1)} \tag{4.1}$$

The sample size to estimate the parameters in the proposed deformation-diffusivity model has been taken to be three. It has been reported that $D_0 = 7.26 \times 10^{-13}$ m^2/s for glass fibers by [49]. Based on the chosen sample size and value of D_0, the estimated diffusivity parameters are given as follows:

$$\eta_T = 1.43 \times 10^4,\ D_T = 23.39 \times 10^{-13}\ \mathrm{m}^2/\mathrm{s},\ E_{\mathrm{ref}_T} = 1.833 \times 10^{-3} \tag{4.2}$$

Using the experimental data reported in [50] under compressive and shear strains, and following a similar procedure as before, the following diffusivity parameters are obtained:

$$\eta_C = 401.19,\ D_C = 8.66 \times 10^{-13}\ \mathrm{m}^2/\mathrm{s},\ E_{\mathrm{ref}_C} = 1.0 \times 10^{-3} \tag{4.3a}$$

$$\eta_S = -239.61,\ D_S = 8.65 \times 10^{-13}\ \mathrm{m}^2/\mathrm{s},\ E_{\mathrm{ref}_S} = 3.0 \times 10^{-3} \tag{4.3b}$$

We then compared the proposed model (which is obtained based on sample size of 3 points) with the experimental data set of 10 points. Figure 4 shows the relation between the relative diffusion coefficient D/D_0 and various strain invariants. From this figure, it is evident that the proposed model is in a good agreement

Table 2 A statistical analysis of the fit

Sample size	Mean data			Standard deviation data			Coefficient of determination		
	Tension	Compression	Shear	Tension	Compression	Shear	Tension	Compression	Shear
10	1.507	1.093	1.114	0.526	0.073	0.068	0.988	0.999	0.997
25	1.505	1.094	1.108	0.511	0.062	0.065	0.986	0.999	0.997
50	1.521	1.095	1.107	0.515	0.062	0.062	0.987	0.999	0.997
75	1.391	1.097	1.115	0.468	0.062	0.059	0.984	0.999	0.997

This table provides the goodness of fit of the proposed model with the experimental data set reported in [49,50]. Analysis is performed for various extracted sample sizes and under tension, compression, and shear strains. It is observed that the coefficient of determination is close to unity

with the experimental data. Table 2 provides a statistical analysis on the fit of the experimental data with the proposed model. The coefficient of determination is close to unity. This means that the proposed model based on parameter set given by Eqs. (4.2)–(4.3b) is a good fit to the set of experimental data of various sample sizes. To calibrate $\mathbf{D}_{MS}$, η_{MS}, and $E_{\mathrm{ref}\,MS}$, we need additional experimental data related to mode of shear. However, such a data set to calibrate the effect of distortion due to shear on the diffusivity of glass is currently not available in the literature. Therefore, we did not calibrate $\mathbf{D}_{MS}$, η_{MS}, and $E_{\mathrm{ref}\,MS}$. However, one can calibrate these parameters in a similar fashion as discussed earlier once the required experimental data are available.

5 Initial boundary value problem and mathematical analysis

From the above statements, the governing equations for the proposed chemo–thermo–mechano degrading model are stated as follows. Let the boundary of $\Omega_0(\mathfrak{B})$ be denoted as $\partial\Omega_0$ and the corresponding unit outward normal to this boundary be denoted by $\widehat{\mathbf{n}}_0(\mathbf{p})$. Similarly, $\partial\Omega_t$ denotes the boundary of $\Omega_t(\mathfrak{B})$ and the corresponding unit outward normal to this boundary is denoted by $\widehat{\mathbf{n}}(\mathbf{x}, t)$. For the deformation subproblem, the boundary is divided into two complementary parts: Γ_u^{D} and Γ_u^{N} such that $\Gamma_u^{\mathrm{D}} \cup \Gamma_u^{\mathrm{N}} = \partial\Omega_0$ and $\Gamma_u^{\mathrm{D}} \cap \Gamma_u^{\mathrm{N}} = \emptyset$. Γ_u^{D} is the part of the boundary on which displacement is prescribed and Γ_u^{N} is the part of the boundary on which traction is prescribed.

Similarly, for the transport and thermal subproblem, the boundary is divided into complementary parts: Γ_c^{D} and Γ_c^{N} and $\Gamma_\vartheta^{\mathrm{D}}$ and $\Gamma_\vartheta^{\mathrm{N}}$ such that $\Gamma_c^{\mathrm{D}} \cup \Gamma_c^{\mathrm{N}} = \partial\Omega_0$, $\Gamma_\vartheta^{\mathrm{D}} \cup \Gamma_\vartheta^{\mathrm{N}} = \partial\Omega$, $\Gamma_c^{\mathrm{D}} \cap \Gamma_c^{\mathrm{N}} = \emptyset$, and $\Gamma_\vartheta^{\mathrm{D}} \cap \Gamma_\vartheta^{\mathrm{N}} = \emptyset$. Γ_c^{D} is the part of the boundary on which concentration is prescribed. Γ_c^{N} is the part of the boundary on which total/diffusive flux is prescribed. $\Gamma_\vartheta^{\mathrm{D}}$ is the part of the boundary on which temperature is prescribed. $\Gamma_\vartheta^{\mathrm{N}}$ is the part of the boundary on which thermal flux is prescribed. In case of steady-state analysis, it should be noted that the meas $\left(\Gamma_c^{\mathrm{D}}\right) > 0$, meas $\left(\Gamma_\vartheta^{\mathrm{D}}\right) > 0$, and meas $\left(\Gamma_u^{\mathrm{D}}\right) > 0$. However, such a condition is not required for studying transient problems.

5.1 Governing equations of the proposed model

The governing equations for the *deformation subproblem* take the following form:

$$\rho_0 \dot{\mathbf{v}}(\mathbf{p}, t) = \mathrm{Div}[\mathbf{P}] + \rho_0 \mathbf{b}(\mathbf{p}, t) \quad \text{in } \Omega_0 \times]0, \mathcal{I}[\tag{5.1a}$$

$$\mathbf{u}(\mathbf{p}, t) = \mathbf{u}^{\mathrm{p}}(\mathbf{p}, t) \quad \text{on } \Gamma_u^{\mathrm{D}} \times]0, \mathcal{I}[\tag{5.1b}$$

$$\mathbf{P}\widehat{\mathbf{n}}_0(\mathbf{p}) = \mathbf{t}^{\mathrm{p}}(\mathbf{p}, t) \quad \text{on } \Gamma_u^{\mathrm{N}} \times]0, \mathcal{I}[\tag{5.1c}$$

$$\mathbf{u}(\mathbf{p}, t = 0) = \mathbf{u}^{\mathrm{i}}(\mathbf{p}) \quad \text{in } \Omega_0 \tag{5.1d}$$

$$\mathbf{v}(\mathbf{p}, t = 0) = \mathbf{v}^{\mathrm{i}}(\mathbf{p}) \quad \text{in } \Omega_0 \tag{5.1e}$$

where $\mathbf{u}^{\mathrm{p}}(\mathbf{p}, t)$ denotes the prescribed displacement on the boundary and $\mathbf{t}^{\mathrm{p}}(\mathbf{p}, t)$ is the prescribed traction on the boundary. $\mathbf{u}^{\mathrm{i}}(\mathbf{p})$ and $\mathbf{v}^{\mathrm{i}}(\mathbf{p})$ are the initial conditions for the displacement and velocity, respectively.

The governing equations for the *transport subproblem* take the following form:

$$\rho_0 \dot{c}(\mathbf{p}, t) + \mathrm{Div}[\mathbf{h}_0] = h_0(\mathbf{p}, t) \quad \text{in } \Omega_0 \times]0, \mathcal{I}[\tag{5.2a}$$

$$c(\mathbf{p}, t) = c^{\mathrm{p}}(\mathbf{p}, t) \quad \text{on } \Gamma_c^{\mathrm{D}} \times]0, \mathcal{I}[\tag{5.2b}$$

$$\mathbf{h}_0 \bullet \widehat{\mathbf{n}}_0(\mathbf{p}) = h^{\mathrm{p}}(\mathbf{p}, t) \qquad \text{on } \Gamma_c^{\mathrm{N}} \times]0, \mathcal{I}[\tag{5.2c}$$

$$c(\mathbf{p}, t = 0) = c^{\mathrm{i}}(\mathbf{p}) \qquad \text{in } \Omega_0 \tag{5.2d}$$

where $c^{\mathrm{p}}(\mathbf{p}, t)$ denotes the prescribed concentration on the boundary, $h^{\mathrm{p}}(\mathbf{p}, t)$ is the prescribed total/diffusive flux on the boundary, and $c^{\mathrm{i}}(\mathbf{p})$ is the initial condition for the concentration field.

The governing equations for the *thermal subproblem* take the following form:

$$\rho_0 \vartheta(\mathbf{p}, t)\dot{\eta} = -\mathrm{Div}[\mathbf{q}_0] - \mathrm{Grad}[\varkappa] \bullet \mathbf{h}_0 + q_0(\mathbf{p}, t) \qquad \text{in } \Omega_0 \times]0, \mathcal{I}[\tag{5.3a}$$

$$\vartheta(\mathbf{p}, t) = \vartheta^{\mathrm{p}}(\mathbf{p}, t) \qquad \text{on } \Gamma_\vartheta^{\mathrm{D}} \times]0, \mathcal{I}[\tag{5.3b}$$

$$\mathbf{q}_0 \bullet \widehat{\mathbf{n}}_0(\mathbf{p}) = q^{\mathrm{p}}(\mathbf{p}, t) \qquad \text{on } \Gamma_c^{\mathrm{N}} \times]0, \mathcal{I}[\tag{5.3c}$$

$$\vartheta(\mathbf{p}, t = 0) = \vartheta^{\mathrm{i}}(\mathbf{p}) \qquad \text{in } \Omega_0 \tag{5.3d}$$

where $\vartheta^{\mathrm{p}}(\mathbf{p}, t)$ denotes the prescribed temperature on the boundary, $q^{\mathrm{p}}(\mathbf{p}, t)$ is the prescribed heat flux on the boundary, and $\vartheta^{\mathrm{i}}(\mathbf{p})$ is the initial condition for the temperature field.

5.2 On the stability of unsteady solutions

We now show that the unsteady solutions under the proposed mathematical model for degradation are stable in the sense of a dynamical system. There are different notions of stability, and herein we shall establish the stability in the sense of Lyapunov [22]. For the entire analysis presented in this section, we assume homogeneous Dirichlet boundary conditions on the entire boundary for the diffusion and thermal subproblems. Let

$$\boldsymbol{\chi} := \left\{ \begin{array}{c} \boldsymbol{\varphi} \\ \mathbf{v} \\ \vartheta \\ c \end{array} \right\} \tag{5.4}$$

Consider the following functional, which is defined on the reference configuration:

$$\mathbb{V}(\boldsymbol{\chi}) := \int\limits_{\Omega_0(\mathfrak{B})} \rho_0 \left(A + \vartheta\eta + \frac{1}{2}\mathbf{v} \bullet \mathbf{v} \right) \mathrm{d}\Omega_0 + \Pi_{\mathrm{mech,ext}}(\boldsymbol{\varphi}) \tag{5.5}$$

where $\Pi_{\mathrm{mech,ext}}(\boldsymbol{\varphi})$ is the potential energy due to external mechanical loading, which is assumed to be conservative. This implies the following

$$\frac{\mathrm{d}}{\mathrm{d}t}\Pi_{\mathrm{mech,ext}}(\boldsymbol{\varphi}) = -\int\limits_{\Omega_0(\mathfrak{B})} \rho_0 \mathbf{b} \bullet \mathbf{v} \, \mathrm{d}\Omega_0 - \int\limits_{\Gamma_u^{\mathrm{N}}} \mathbf{t}^{\mathrm{p}} \bullet \mathbf{v} \, \mathrm{d}\Gamma_0 \tag{5.6}$$

In the literature, the above functional has been shown to be a Lyapunov functional for linearized thermoelasticity and for thermo-hyperelasticity. For example, see [17,23,30] and references therein. Herein, we shall show that the above functional is a legitimate Lyapunov functional for the proposed degradation model, and specifically use the Lyapunov's second method for stability (which is a classical result in the theory of dynamical systems; e.g., see [31,70,80]) to establish the stability of the solutions under the proposed degradation model.

To this end, we shall take the reference or equilibrium state as:

$$\boldsymbol{\chi}_{\mathrm{eq}} := \left\{ \begin{array}{c} \boldsymbol{\varphi}_{\mathrm{eq}} \\ \mathbf{0} \\ 0 \\ 0 \end{array} \right\} \tag{5.7}$$

where $\boldsymbol{\varphi}_{\mathrm{eq}}$ is the static equilibrium deformation. The above functional is a candidate for Lyapunov functional, as it satisfies:

$$\mathbb{V}(\boldsymbol{\chi} = \boldsymbol{\chi}_{\mathrm{eq}}) = 0 \quad \text{and} \quad \mathbb{V}(\boldsymbol{\chi} \neq \boldsymbol{\chi}_{\mathrm{eq}}) > 0 \tag{5.8}$$

We now show that $\frac{\mathrm{d}\mathbb{V}}{\mathrm{d}t} \leq 0$. Let us start by writing:

$$\begin{aligned}
\frac{\mathrm{d}\mathbb{V}}{\mathrm{d}t} &= \int\limits_{\Omega_0(\mathfrak{B})} \rho_0 \left(\frac{\partial A}{\partial \mathbf{F}} \bullet \dot{\mathbf{F}} + \frac{\partial A}{\partial \vartheta}\dot{\vartheta} + \frac{\partial A}{\partial c}\dot{c} + \dot{\vartheta}\eta + \vartheta\dot{\eta} + \mathbf{v} \bullet \dot{\mathbf{v}} \right) \mathrm{d}\Omega_0 + \frac{\mathrm{d}}{\mathrm{d}t}\Pi_{\mathrm{mech,ext}}(\boldsymbol{\varphi}) \\
&= \int\limits_{\Omega_0(\mathfrak{B})} \rho_0 \left(\varkappa\dot{c} + \vartheta\dot{\eta}\right) \mathrm{d}\Omega_0 + \int\limits_{\Omega_0(\mathfrak{B})} \rho_0 \left(\frac{\partial A}{\partial \vartheta} + \eta \right) \dot{\vartheta} \, \mathrm{d}\Omega_0 + \int\limits_{\Omega_0(\mathfrak{B})} \left(\rho_0 \mathbf{v} \bullet \dot{\mathbf{v}} + \mathbf{P} \bullet \dot{\mathbf{F}} \right) \mathrm{d}\Omega_0 + \frac{\mathrm{d}}{\mathrm{d}t}\Pi_{\mathrm{mech,ext}}(\boldsymbol{\varphi}) \\
&= \int\limits_{\Omega_0(\mathfrak{B})} \rho_0 \left(\varkappa\dot{c} + \vartheta\dot{\eta}\right) \mathrm{d}\Omega_0 \\
&= -\int\limits_{\Omega_0(\mathfrak{B})} \varkappa \mathrm{Div}[\mathbf{h}_0] \, \mathrm{d}\Omega_0 - \int\limits_{\Omega_0(\mathfrak{B})} \frac{\vartheta - \vartheta_{\mathrm{ref}}}{\vartheta} \mathrm{Div}[\mathbf{q}_0] \, \mathrm{d}\Omega_0 - \int\limits_{\Omega_0(\mathfrak{B})} \frac{\vartheta - \vartheta_{\mathrm{ref}}}{\vartheta} \mathrm{Grad}[\varkappa] \bullet \mathbf{h}_0 \, \mathrm{d}\Omega_0 \\
&= \int\limits_{\Omega_0(\mathfrak{B})} \mathrm{Grad}[\varkappa] \bullet \mathbf{h}_0 \, \mathrm{d}\Omega_0 - \int\limits_{\Omega_0(\mathfrak{B})} \left(1 - \frac{\vartheta_{\mathrm{ref}}}{\vartheta}\right) \mathrm{Div}[\mathbf{q}_0] \, \mathrm{d}\Omega_0 - \int\limits_{\Omega_0(\mathfrak{B})} \left(1 - \frac{\vartheta_{\mathrm{ref}}}{\vartheta}\right) \mathrm{Grad}[\varkappa] \bullet \mathbf{h}_0 \, \mathrm{d}\Omega_0 \\
&= \int\limits_{\Omega_0(\mathfrak{B})} \frac{\vartheta_{\mathrm{ref}}}{\vartheta} \left(\frac{1}{\vartheta} \mathrm{Grad}[\vartheta] \bullet \mathbf{q}_0 + \mathrm{Grad}[\varkappa] \bullet \mathbf{h}_0 \right) \mathrm{d}\Omega_0 = -\int\limits_{\Omega_0(\mathfrak{B})} \frac{\vartheta_{\mathrm{ref}}}{\vartheta} \zeta_0 \, \mathrm{d}\Omega_0
\end{aligned} \tag{5.9}$$

Since $\zeta_0 > 0$ if $\boldsymbol{\chi} \neq \boldsymbol{\chi}_{\mathrm{eq}}$, $\vartheta,\ \vartheta_{\mathrm{ref}} > 0$, one can conclude that

$$\frac{\mathrm{d}\mathbb{V}}{\mathrm{d}t} < 0 \tag{5.10}$$

From the Lyapunov stability of continuous systems [22,31], one can conclude that $\boldsymbol{\chi} = \boldsymbol{\chi}_{\mathrm{eq}}$ is asymptotically stable.

6 Semi-analytical solutions to canonical problems

In this section, we shall appeal to semi-inverse methods to obtain solutions to some popular canonical boundary value problems [56]. Incompressible neo-Hookean chemo–thermo–mechano degradation model is considered here. Similar analysis can be performed for other compressible and incompressible chemo-mechano, thermo-mechano, and chemo–thermo–mechano degradation models. Coordinate system under consideration is either spherical or cylindrical. In all the problems discussed below, we assume concentration and temperature to be functions of time t and radius r (which is a current configuration variable). This assumption is often made because the underlying problem has either cylindrical or spherical symmetry. We also assume that the volumetric sources corresponding to temperature and concentration are equal to zero. In this paper, as we are mainly interested in degradation of solid due to temperature and transport of chemical species, we shall neglect Dufour effect, Soret effect, thermo-chemo coupling parameter $d_{\vartheta c}$, and anisotropic coefficient of thermal and chemical expansions. In order to reduce the complexity of finding solutions based on semi-inverse method for deformation subproblem, we shall neglect the inertial effects and body forces.

Based on the assumptions provided here, the governing equations for the transport subproblem in cylindrical coordinates reduce to:

$$\rho \frac{\partial c}{\partial t} + \frac{1}{r}\frac{\partial r h_r}{\partial r} = 0,\ c(r = r_i, t) = c_i,\ c(r = r_o, t) = c_o,\ c(r, t = 0) = c_0 \tag{6.1}$$

where h_r is the mass transfer flux in the radial direction. Similarly, the governing equations for the thermal subproblem in cylindrical coordinates can be written as:

$$\rho\vartheta \frac{\partial \eta}{\partial t} + \frac{1}{r}\frac{\partial r q_r}{\partial r} = -\frac{\partial \varkappa}{\partial r} h_{\mathrm{r}},\ \vartheta(r = r_i, t) = \vartheta_i,\ \vartheta(r = r_o, t) = \vartheta_o,\ \vartheta(r, t = 0) = \vartheta_0 \tag{6.2}$$

where q_r is the heat flux in the radial direction. In spherical coordinates, the governing equations for the transport subproblem are:

$$\rho\frac{\partial c}{\partial t}+\frac{1}{r^2}\frac{\partial r^2 h_r}{\partial r}=0,\ c(r=r_i,t)=c_i,\ c(r=r_o,t)=c_o,\ c(r,t=0)=c_0 \tag{6.3}$$

The governing equations for the thermal subproblem in spherical coordinates are:

$$\rho\vartheta\frac{\partial \eta}{\partial t}+\frac{1}{r^2}\frac{\partial r^2 q_r}{\partial r}=-\frac{\partial \varkappa}{\partial r}h_{\mathrm{r}},\ \vartheta(r=r_i,t)=\vartheta_i,\ \vartheta(r=r_o,t)=\vartheta_o,\ \vartheta(r,t=0)=\vartheta_0 \tag{6.4}$$

Another quantity of interest in material degradation is the extent of damage at a particular location or along the cross section of the degrading body. In case of incompressible neo-Hookean chemo–thermo–mechano degradation model, this quantity can be defined as follows:

$$\mathcal{D}_\mu(\mathbf{x},t):=\frac{\mu}{\mu_0}=1-\left(\frac{\mu_1 c}{\mu_0 c_{\mathrm{ref}}}\right)-\left(\frac{\mu_2\vartheta}{\mu_0\vartheta_{\mathrm{ref}}}\right) \tag{6.5}$$

For virgin material, $\mathcal{D}_\mu=1$. If $\mathcal{D}_\mu$ approaches zero, then the material has degraded the most. In addition, Eq. (6.5) also provides the following information:

- Amount of degradation at a given location and time,
- The parts of the body that suffered extensive damage, and
- The effect of temperature and moisture (or concentration of chemical species) on the mechanical properties of materials.

6.1 Inflation of a degrading spherical shell

We now study the behavior of a degrading (thick) spherical shell subjected to pressure loading. Figure 5 provides a pictorial description of the boundary value problem. In addition to the obvious theoretical significance, this problem has relevance to safety, reliability, and defect monitoring of degrading spherical structures (such as a tank shell and a bearing structure) due to pressure loading.

Due to the spherical symmetry of the problem, spherical coordinates are used to analyze the inflation of degrading spherical shell. Consider a spherical body of inner radius R_i and outer radius R_o defined in the reference configuration as follows:

$$R_i\le R\le R_o,\quad 0\le\Theta\le\pi,\quad 0\le\Phi\le 2\pi \tag{6.6}$$

where (R,Θ,Φ) are the spherical polar coordinates in the reference configuration. The inner and outer surfaces $R=R_i$ and $R=R_o$ are, respectively, subjected to pressures p_i and p_o with $p_i\ge p_o$. That is, the thick cylinder is inflated with pressure. The deformation in the current configuration can be described as follows:

$$r_i\le r=m(R)\le r_o,\quad \theta=\Theta,\quad \phi=\Phi \tag{6.7}$$

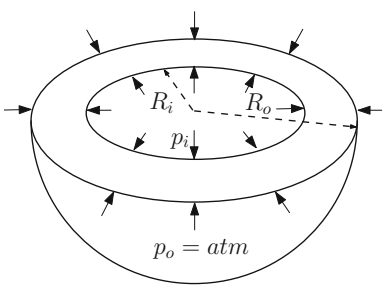

Fig. 5 Inflation of a degrading spherical shell: A pictorial description of degrading shell in the reference configuration. The shell is subjected to an inner pressure p_i and an outer pressure p_o

where (r, θ, ϕ) are the spherical polar coordinates in the current configuration and r_i and r_o are, respectively, the inner and outer radii of the shell in the current (deformed) configuration. The deformation gradient, the left Cauchy–Green tensor, and the right Cauchy–Green tensor have the following matrix representations:

$$\{\mathbf{F}\} = \begin{pmatrix} \frac{\mathrm{d}m}{\mathrm{d}R} & 0 & 0 \\ 0 & \frac{m}{R} & 0 \\ 0 & 0 & \frac{m}{R} \end{pmatrix}, \quad \{\mathbf{C}\} = \{\mathbf{B}\} = \begin{pmatrix} \left(\frac{\mathrm{d}m}{\mathrm{d}R}\right)^2 & 0 & 0 \\ 0 & \frac{m^2}{R^2} & 0 \\ 0 & 0 & \frac{m^2}{R^2} \end{pmatrix} \tag{6.8}$$

Incompressibility implies that

$$r = m(R) = \sqrt[3]{R^3 + r_i^3 - R_i^3} \qquad r_i \le r \le r_o \tag{6.9}$$

where $r_o = \sqrt[3]{R_o^3 + r_i^3 - R_i^3}$. The nonzero components of the Cauchy stress are:

$$T_{rr} = -p + \mu(c, \vartheta)\left(\frac{\mathrm{d}m}{\mathrm{d}R}\right)^2 = -p + \mu(c, \vartheta)\frac{R^4}{r^4}, \quad T_{\theta\theta} = T_{\phi\phi} = -p + \mu(c, \vartheta)\frac{r^2}{R^2} \tag{6.10}$$

The governing equations for the balance of linear momentum in the spherical polar coordinates (e.g., see [65]) reduce to:

$$\frac{\partial T_{rr}}{\partial r} + \frac{2T_{rr} - T_{\theta\theta} - T_{\phi\phi}}{r} = 0, \ \frac{\partial p}{\partial \theta} = 0, \ \frac{\partial p}{\partial \phi} = 0 \tag{6.11}$$

The above equations imply that p is independent of θ and ϕ. That is,

$$p = p(r, t) \tag{6.12}$$

From Eqs. (3.6) and (3.7), the specific chemical potential and specific entropy for the degrading spherical shell are given as follows:

$$\varkappa = \frac{1}{\rho_0}\frac{\partial \psi}{\partial c} + R_s\vartheta_{\mathrm{ref}}\{c - c_{\mathrm{ref}}\} = -\frac{\mu_1}{2\rho_0 c_{\mathrm{ref}}}\left(\frac{R^4}{r^4} + 2\frac{r^2}{R^2} - 3\right) + R_s\vartheta_{\mathrm{ref}}\{c - c_{\mathrm{ref}}\} \tag{6.13a}$$

$$\eta = -\frac{1}{\rho_0}\frac{\partial \psi}{\partial \vartheta} + \frac{c_p}{\vartheta_{\mathrm{ref}}}\{\vartheta - \vartheta_{\mathrm{ref}}\} = \frac{\mu_1}{2\rho_0\vartheta_{\mathrm{ref}}}\left(\frac{R^4}{r^4} + 2\frac{r^2}{R^2} - 3\right) + \frac{c_p}{\vartheta_{\mathrm{ref}}}\{\vartheta - \vartheta_{\mathrm{ref}}\} \tag{6.13b}$$

Before deriving the governing equations for the degrading shell problem, we shall do the non-dimensionalization by choosing primary variables and associated reference quantities that are convenient for studying this problem. To distinguish, we shall denote all the non-dimensional quantities using a superposed bar. We shall take μ_0, R_o, ϑ_{ref}, c_{ref}, and D_0 as the reference quantities, which give rise to the following non-dimensional quantities:

$$\overline{r} = \frac{r}{R_o}, \ \overline{R} = \frac{R}{R_o}, \ \overline{D}_{\varkappa\varkappa} = \frac{D_{\varkappa\varkappa}}{D_0}, \ \overline{D}_{\vartheta\vartheta} = \frac{D_{\vartheta\vartheta}}{D_0} \tag{6.14}$$

$$\overline{\mu}_1 = \frac{\mu_1}{\mu_0}, \ \overline{\mu}_2 = \frac{\mu_2}{\mu_0}, \ \overline{c} = \frac{c}{c_{\mathrm{ref}}}, \ \overline{\vartheta} = \frac{\vartheta}{\vartheta_{\mathrm{ref}}}, \ \overline{t} = \frac{D_0 t}{R_o^2} \tag{6.15}$$

With the stress field in Eq. (6.10), we shall integrate Eq. (6.11) and then have the following nonlinear equation in deformation subproblem after non-dimensionalization:

$$\overline{T}_{rr}(\overline{R} = \overline{R}_i, \overline{t}) - \overline{T}_{rr}(\overline{R} = \overline{R}_o, \overline{t}) = \overline{p}_o - \overline{p}_i = \int_{\overline{R}_i}^{\overline{R}_o} \frac{2\overline{\mu}(\overline{c}, \overline{\vartheta})\left(\overline{R}^6 - \left(\overline{R}^3 + \overline{r}_i^3 - \overline{R}_i^3\right)^2\right)}{\left(\overline{R}^3 + \overline{r}_i^3 - \overline{R}_i^3\right)^{\frac{7}{3}}}\mathrm{d}\overline{R} \tag{6.16}$$

In order to reduce the complexity in finding semi-analytical solutions, we shall assume $\frac{\partial r}{\partial t} \ll \frac{\partial \vartheta}{\partial t}$. Substituting Eqs. (6.13a) and (6.13b) into the constitutive relations of the proposed model, the governing equations of these two subproblems (6.3), (6.4) can be written as follows after non-dimensionalization:

$$\frac{\partial \overline{c}}{\partial \overline{t}} - \left(\frac{2\overline{D}_{\varkappa\varkappa}}{\overline{r}} + \frac{\partial \overline{D}_{\varkappa\varkappa}}{\partial \overline{r}}\right)\frac{\partial \overline{c}}{\partial \overline{r}} - \overline{D}_{\varkappa\varkappa}\frac{\partial^2 \overline{c}}{\partial \overline{r}^2} = 2\overline{\omega}\frac{\partial \overline{D}_{\varkappa\varkappa}}{\partial \overline{r}}\left(\frac{\overline{R}^4}{\overline{r}^5} - \frac{\overline{r}}{\overline{R}^2}\right) - 6\overline{\omega}\overline{D}_{\varkappa\varkappa}\left(\frac{1}{\overline{R}^2} + \frac{\overline{R}^4}{\overline{r}^6}\right) \tag{6.17}$$

$$\overline{\vartheta}\frac{\partial \overline{\vartheta}}{\partial \overline{t}} - \left(2\frac{\overline{D}_{\vartheta\vartheta}}{\overline{r}} + \frac{\partial \overline{D}_{\vartheta\vartheta}}{\partial \overline{r}}\right)\frac{\partial \overline{\vartheta}}{\partial \overline{r}} - \overline{D}_{\vartheta\vartheta}\frac{\partial^2 \overline{\vartheta}}{\partial \overline{r}^2} = \overline{\tau}\overline{D}_{\varkappa\varkappa}\left(\frac{\partial \overline{c}}{\partial \overline{r}} - 2\overline{\omega}\left(\frac{\overline{r}}{\overline{R}^2} - \frac{\overline{R}^4}{\overline{r}^5}\right)\right)^2 \tag{6.18}$$

where $\overline{\omega}$ and $\overline{\tau}$ are two non-dimensional parameters, which have the following expressions:

$$\overline{\omega} = \frac{\mu_1}{\rho_0 R_s \vartheta_{\text{ref}} c_{\text{ref}}^2}, \quad \overline{\tau} = \frac{R_s c_{\text{ref}}^2}{c_p} \tag{6.19}$$

These two non-dimensional parameters can show the strength of coupling effect in chemical potential and specific entropy. The nonlinear equation (6.16) enables us to find $\overline{r}_i$ at various $\overline{t}$ for given $\overline{c}(\overline{R}, \overline{t})$ and $\overline{\vartheta}(\overline{R}, \overline{t})$. However, it should be noted that $\overline{c}(\overline{R}, \overline{t})$ and $\overline{\vartheta}(\overline{R}, \overline{t})$ are also a function of $\overline{r}_i$ in case of strong coupling. This is because diffusivity and thermal conductivity depend on the invariants of strain $\overline{\mathbf{E}}$. Hence, the integral equation (6.16) and partial differential equations (6.17) and (6.18) are strongly coupled. By strong coupling, we mean that diffusivity and thermal conductivity depend on the mechanical deformation, and by weak coupling, we mean that the diffusivity and thermal conductivity do not depend on strain or stress. The selection of strong versus weak coupling depends on material properties. In general, a systematic sensitivity analysis is required to offer a concrete guidance criterion (e.g., variance-based or distance-based global sensitivity analysis [66,67]), which is beyond the scope of this paper.

6.1.1 Steady-state analysis for shell degradation

For steady state, we have $h_r r^2 = C_1$ and $q_r r^2 + \varkappa h_r r^2 = C_2$, where C_1 and C_2 are integration constants. This implies that $\overline{c}$ and $\overline{\vartheta}$ are the solutions of the following ODEs:

$$\overline{D}_{\varkappa\varkappa}\overline{r}^2\frac{\mathrm{d}\overline{c}}{\mathrm{d}\overline{r}} - 2\overline{D}_{\varkappa\varkappa}\overline{\omega}\left(\frac{\overline{r}^3}{\overline{R}^2} - \frac{\overline{R}^4}{\overline{r}^3}\right) + \overline{C}_1 = 0 \tag{6.20a}$$

$$\overline{D}_{\vartheta\vartheta}\overline{r}^2\frac{\mathrm{d}\overline{\vartheta}}{\mathrm{d}\overline{r}} + \overline{\tau}\left(\frac{\overline{w}}{2}\left(\frac{\overline{R}^4}{\overline{r}^4} + 2\frac{\overline{r}^2}{\overline{R}^2} - 3\right) - \overline{c} + 1\right)\overline{C}_1 + \overline{C}_2 = 0 \tag{6.20b}$$

where the integration constants $\overline{C}_1$ and $\overline{C}_2$ are determined from the boundary conditions for the transport and thermal subproblems. Under weak coupling (i.e., $D_{\vartheta\vartheta}$ and $D_{\varkappa\varkappa}$ are constants), a simplified form of the analytical solutions for $\overline{c}$ and $\overline{\vartheta}$ can be obtained as follows:

$$\overline{c} = \overline{\omega}\left(\frac{\overline{r}^2}{\overline{R}^2} + \frac{\overline{R}^4}{2\overline{r}^4}\right) + \frac{B_1}{\overline{r}} + A_1, \quad \overline{\vartheta} = -\frac{\overline{\tau}B_1^2\overline{D}_{\varkappa\varkappa}}{2\overline{D}_{\vartheta\vartheta}\overline{r}^2} + \frac{Z_1}{\overline{r}} + Y_1 \tag{6.21}$$

where A_1, B_1, Y_1, and Z_1 are constants, which are given in terms of the boundary conditions $\overline{c}_i$, $\overline{c}_o$, $\overline{\vartheta}_i$, and $\overline{\vartheta}_o$ as follows:

$$A_1 = \overline{c}_i - \frac{B_1}{\overline{r}_i} - \overline{\omega}\left(\frac{\overline{r}_i^2}{\overline{R}^2} + \frac{8\overline{R}^4}{\overline{r}_i^4}\right) \tag{6.22a}$$

$$B_1 = \frac{\overline{r}_i\overline{r}_o}{\overline{r}_i - \overline{r}_o}\left(\overline{c}_o - \overline{c}_i - \overline{\omega}\left(\frac{\overline{r}_o^2}{\overline{R}^2} + \frac{8\overline{R}^4}{\overline{r}_o^4} - \frac{\overline{r}_i^2}{\overline{R}^2} - \frac{8\overline{R}^4}{\overline{r}_i^4}\right)\right) \tag{6.22b}$$

$$Y_1 = \overline{\vartheta}_i + \frac{\overline{\tau}B_1^2\overline{D}_{\varkappa\varkappa}}{2\overline{D}_{\vartheta\vartheta}\overline{r}_i^2} - \frac{Z_1}{\overline{r}_i} \tag{6.22c}$$

$$Z_1 = \frac{\overline{r}_i - \overline{r}_o}{\overline{r}_i \overline{r}_o}\left(\overline{\vartheta}_o - \overline{\vartheta}_i - \frac{\overline{\tau} B_1^2 \overline{D}_{\varkappa\varkappa}}{2\overline{D}_{\vartheta\vartheta}}\left(\frac{1}{\overline{r}_i^2} - \frac{1}{\overline{r}_o^2}\right)\right) \tag{6.22d}$$

6.1.2 Unsteady analysis for shell degradation

Herein, we shall integrate Eq. (6.16) using trapezoidal rule (`trapz` function in MATLAB [47]). The method of horizontal lines [60,64] and shooting method [33] are used to obtain numerical solutions to Eqs. (6.17) and (6.18). In the method of horizontal lines, the time is discretized first followed by spatial discretization. The time interval of interest $[0, \overline{\mathcal{T}}]$ is divided into N non-overlapping subintervals such that $\Delta\bar{t} = \frac{\overline{\mathcal{T}}}{N}$ and $\bar{t}_n = n\Delta\bar{t}$. $\bar{t}_n$ is called the integral time level, where $n = 0, \ldots, N$. $\Delta\bar{t}$ is the time step, which is assumed to be uniform. Employing the method of horizontal lines with backward Euler time-stepping scheme, we obtain the following ODEs at each time level for Eqs. (6.17) and (6.18):

$$\begin{aligned}
&\frac{\mathrm{d}^2\overline{c}^{(n+1)}}{\mathrm{d}\overline{r}^2} + \left(\frac{2}{\overline{r}^{(n)}} + \left(\frac{1}{\overline{D}_{\varkappa\varkappa}^{(n)}}\right)\frac{\mathrm{d}\overline{D}_{\varkappa\varkappa}}{\mathrm{d}\overline{r}}\bigg|_{\bar{t}=\bar{t}_n}\right)\frac{\mathrm{d}\overline{c}^{(n+1)}}{\mathrm{d}\overline{r}} - \frac{\overline{c}^{(n+1)}}{\overline{D}_{\varkappa\varkappa}^{(n)}\Delta\bar{t}} = 6\overline{\omega}\left(\frac{1}{\left(\overline{R}^{(n)}\right)^2} + \frac{\left(\overline{R}^{(n)}\right)^4}{\left(\overline{r}^{(n)}\right)^6}\right) \\
&\quad - \frac{\overline{c}^{(n)}}{\overline{D}_{\varkappa\varkappa}^{(n)}\Delta\bar{t}} - \left(\frac{2\overline{\omega}}{\overline{D}_{\varkappa\varkappa}^{(n)}}\right)\left(\frac{\mathrm{d}\overline{D}_{\varkappa\varkappa}}{\mathrm{d}\overline{r}}\bigg|_{\bar{t}=\bar{t}_n}\right)\left(\frac{\left(\overline{R}^{(n)}\right)^4}{\left(\overline{r}^{(n)}\right)^5} - \frac{\overline{r}^{(n)}}{\left(\overline{R}^{(n)}\right)^2}\right)
\end{aligned} \tag{6.23}$$

$$\begin{aligned}
&\frac{\mathrm{d}^2\overline{\vartheta}^{(n+1)}}{\mathrm{d}\overline{r}^2} + \left(\frac{2}{\overline{r}^{(n)}} + \left(\frac{1}{\overline{D}_{\vartheta\vartheta}^{(n)}}\right)\frac{\mathrm{d}\overline{D}_{\vartheta\vartheta}}{\mathrm{d}\overline{r}}\bigg|_{\bar{t}=\bar{t}_n}\right)\frac{\mathrm{d}\overline{\vartheta}^{(n+1)}}{\mathrm{d}\overline{r}} - \frac{\overline{\vartheta}^{(n)}\overline{\vartheta}^{(n+1)}}{\overline{D}_{\vartheta\vartheta}^{(n)}\Delta\bar{t}} = -\frac{\left(\overline{\vartheta}^{(n)}\right)^2}{\overline{D}_{\vartheta\vartheta}^{(n)}\Delta\bar{t}} \\
&\quad - \frac{\overline{\tau}\overline{D}_{\varkappa\varkappa}^{(n)}}{\overline{D}_{\vartheta\vartheta}^{(n)}}\left(\frac{\mathrm{d}\overline{c}}{\mathrm{d}\overline{r}}\bigg|_{\bar{t}=\bar{t}_n} - 2\overline{\omega}\left(\frac{\left(\overline{r}^{(n)}\right)}{\left(\overline{R}^{(n)}\right)^2} - \frac{\left(\overline{R}^{(n)}\right)^4}{\left(\overline{r}^{(n)}\right)^5}\right)\right)^2
\end{aligned} \tag{6.24}$$

where $\overline{c}^{(n)} = \overline{c}(\overline{r}, \bar{t} = \bar{t}_n)$ and $\overline{\vartheta}^{(n)} = \overline{\vartheta}(\overline{r}, \bar{t} = \bar{t}_n)$. Algorithm 1 describes a procedure to determine $\overline{c}(\overline{r}, \bar{t})$, $\overline{\vartheta}(\overline{r}, \bar{t})$, and r_i at various times using an iterative nonlinear numerical solution strategy. The following values are assumed for the non-dimensional parameters in the strong coupling simulations:

Algorithm 1 Inflation of a degrading spherical shell (numerical methodology to find $\overline{r}_i$, $\overline{c}$, and $\overline{\vartheta}$)

1: INPUT: Non-dimensional material parameters, non-dimensional boundary conditions, and non-dimensional initial conditions, `MaxIters` (which is taken to be equal to 100), tolerances $\epsilon_{\text{tol}}^{(r)}$, $\epsilon_{\text{tol}}^{(c)}$, and $\epsilon_{\text{tol}}^{(\vartheta)}$.
2: Evaluate $\overline{r}_i$ at $\bar{t} = 0$ based on Eq. (6.16).
3: **for** $n = 1, 2, \ldots, N$ **do**
4: **for** $j = 1, 2, \ldots$ **do**
5: **if** $j >$ `MaxIters` **then**
6: Solution did not converge in specified maximum number of iterations. EXIT.
7: **end if**
8: `Diffusion subproblem`: Given $\overline{r}_i^{(j)}$, solve Eq. (6.23) to obtain $\overline{c}^{(j+1)}$. Herein, we use shooting method to solve the ODEs.
9: `Heat conduction subproblem`: Given $\overline{r}_i^{(j)}$ and $\overline{c}^{(j+1)}$, solve Eq. (6.24) to obtain $\overline{\vartheta}^{(j+1)}$. Similarly, we use shooting method to solve the nonlinear ODEs.
10: `Deformation subproblem`: Given $\overline{c}^{(j+1)}$ and $\overline{\vartheta}^{(j+1)}$, solve for $\overline{r}_i^{(j+1)}$ given by Eq. (6.16) using bisection method.
11: **if** $\|\overline{r}_i^{(j+1)} - \overline{r}_i^{(j)}\| < \epsilon_{\text{tol}}^{(r)}$, $\|\overline{c}^{(j+1)} - \overline{c}^{(j)}\| < \epsilon_{\text{tol}}^{(c)}$, and $\|\overline{\vartheta}^{(j+1)} - \overline{\vartheta}^{(j)}\| < \epsilon_{\text{tol}}^{(\vartheta)}$ **then**
12: OUTPUT: $\overline{r}_i^{(j+1)}$, $\overline{c}^{(j+1)}$, and $\overline{\vartheta}^{(j+1)}$. EXIT.
13: **else**
14: Update the guess: $\overline{r}_i^{(j)} \leftarrow \overline{r}_i^{(j+1)}$.
15: **end if**
16: **end for**
17: **end for**

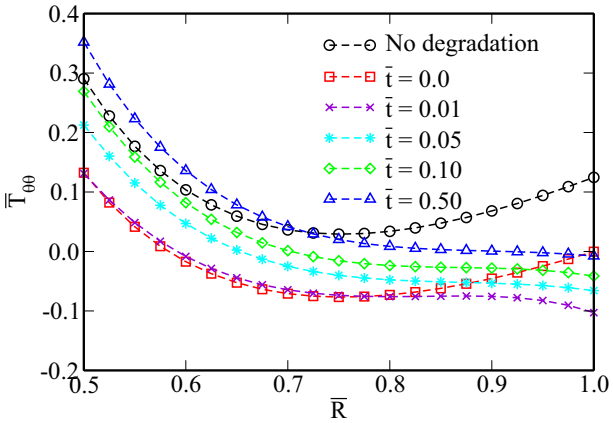

Fig. 6 Inflation of a degrading spherical shell: This figure shows the hoop stress $\overline{T}_{\theta\theta}$ as a function of $\overline{R}$ at various instants of time due to an inner pressure of $\overline{p}_i = 0.5$. Analysis is performed under strongly coupled chemo–thermo–mechano degradation. Note that the stress is increasing with time under degradation

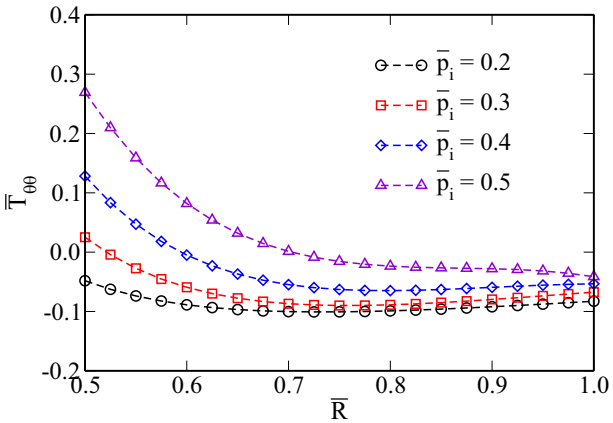

Fig. 7 Inflation of a degrading spherical shell: This figure shows the hoop stress $\overline{T}_{\theta\theta}$ as a function of $\overline{R}$ at $\overline{t} = 0.1$ for various inner pressures $\overline{p}_i$. Analysis is performed for strongly coupled chemo–thermo–mechano degradation. $\overline{T}_{\theta\theta}$ increases in a nonlinear fashion as the pressure loading increases, which is different from the case as time progresses

$$\begin{aligned}
&\overline{R}_o = 1,\ \overline{R}_i = 0.5,\ \Delta\overline{t} = 0.01,\ \overline{t} = 2,\ \overline{\omega} = 0.05,\ \overline{\tau} = 0.2,\ \overline{c}_i = 0, \overline{\vartheta}_0 = 0.5\\
&\overline{c}_o = 1,\ \overline{\vartheta}_i = 0.5,\ \overline{\vartheta}_o = 1,\ \overline{\mu}_0 = 1,\ \overline{\mu}_1 = 0.3,\ \overline{\mu}_2 = 0.4,\ \overline{D}_0 = 1,\ \overline{D}_T = 1.5,\\
&\overline{D}_S = 1.2,\ \eta_T = \eta_S = 1,\ E_{\mathrm{ref}T} = E_{\mathrm{ref}S} = 1,\ \overline{K}_0 = 1,\ \delta = 10
\end{aligned} \tag{6.25}$$

The physical meaning for boundary conditions and initial conditions for this problem is as follows: The body is initially assumed to be in its virgin state and there is no moisture/diffusant/inert chemical species in the body. Also, the body's temperature is constant initially. After time $t = 0$, the inner and outer boundaries of the spherical shell are held at zero and constant concentration. Such a boundary condition can be maintained through a suction/sink mechanism, wherein the moisture/inert species are removed continuously and temperature is held fixed.

In weakly coupling problem, we use $\overline{D}_0$, $\overline{K}_0$ as $\overline{D}^{(n)}_{\varkappa\varkappa}$ and $\overline{D}^{(n)}_{\vartheta\vartheta}$, respectively. It should be noted that these values are constructed based on the (brittle-type) material parameters such as glass, ceramics, and concrete.

The numerical results are shown in Figs. 7, 8, 9, 10 and 11, which reveal the following conclusions on the overall behavior of degrading spherical shells under inflation:

1. Degradation versus non-degradation: After degradation, a spherical shell which is initially homogeneous is not homogeneous anymore, see Fig. 10.

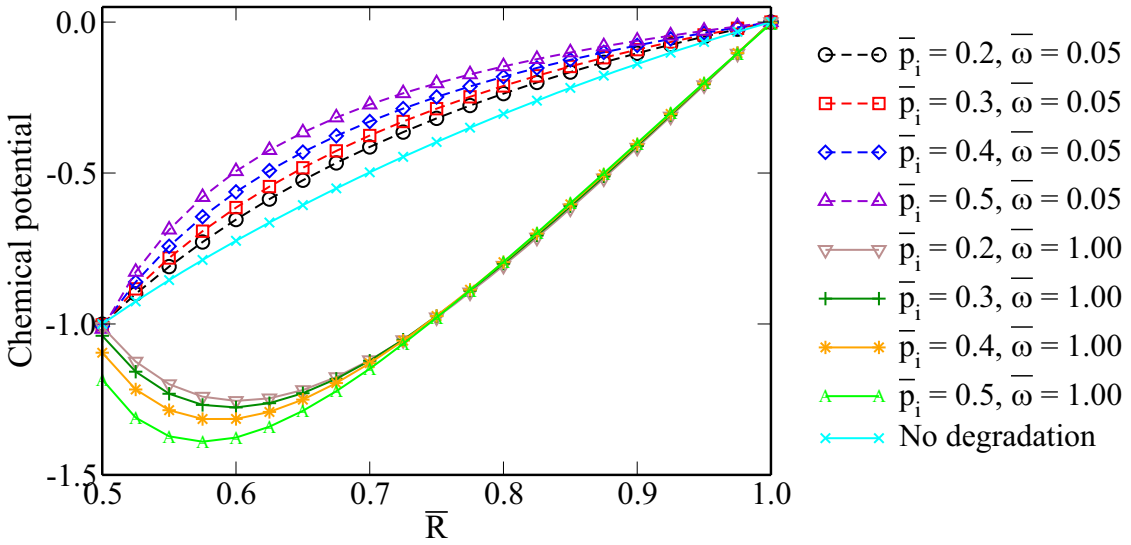

Fig. 8 Inflation of a degrading spherical shell: This figure shows the chemical potential as a function of the reference location $\overline{R}$ at $\overline{t} = 0.2$ due to various inner pressures $\overline{p}_i$ under different cases. One can see that for non-degrading shell, the chemical potential is unchanged with respect to pressure loading. However, for strong coupling, it increases with $\overline{p}_i$ in a nonlinear fashion when non-dimensional parameter $\overline{\omega}$ is small enough. This is because for small $\overline{\omega}$, diffusion takes the dominance in the coupling effect. When pressure loading increases, the diffusivity is increasing due to the growing tr[**E**]. For large $\overline{\omega}$, the deformation is dominant in the coupling, which is $-\overline{I}_E$ term in chemical potential. Since the first invariant $\overline{I}_E$ is always positive in this problem, chemical potential is decreasing when the pressure loading increases

2. Due to degradation, creep-like behavior is observed in Fig. 9. Therefore, as time progresses, hoop stresses increase in Fig. 6. We need to note that the shell ceases to creep after a certain period of time, which is the moment when the transport of chemical species and heat conduction are close to steady states.
3. As the pressure loading increases, the hoop stress is increasing in a nonlinear fashion in Fig. 7, which is significantly different from the non-degradation shell.
4. In Fig. 8, for non-degrading shell, the chemical potential is unchanged with respect to pressure loading. However, for strong coupling, it increases with $\overline{p}_i$ in a nonlinear fashion when $\overline{\omega}$ is small enough. This is because for small $\overline{\omega}$, diffusion takes the dominance in the coupling effect. When pressure loading increases, the diffusivity is increasing due to the growing strain. For large $\overline{\omega}$, the deformation is dominant in the coupling, which is $-\overline{I}_E$ term in chemical potential. Since the first invariant $\overline{I}_E$ is always positive in this problem, chemical potential is decreasing when the pressure loading increases.
5. Thermo-dominated versus chemo-dominated degradation: As Fig. 10 shows, weak coupling over-predicts the amount of degradation compared to the full (or strong) coupling when thermal degradation dominates. This is because when the thermal degradation dominants, the thermal conductivity decreases due to the increase in strain (note that the first invariant of strain is always positive in this problem). However, in chemo-dominated degradation, weak coupling underpredicts the amount of degradation compared to the strong coupling case.
6. In case of strong coupling, healing-like behavior is observed at early time steps in thermo-dominated degradation (but still remains below that of the virgin material), see Fig. 11. This is because of the deformation-dependent thermal diffusivity in the entire body (due to which temperature gets lower than the initial condition). Hence, the material damage is less than that of at $\overline{t} = 0$. However, this heal-like behavior becomes less distinct (or even doesn't exist) when the chemo-degradation achieves the dominance.
7. Strong versus weak coupling: Quantitatively and qualitatively, extent of damage for both strong and weak coupling is considerably different, see Figs. 9, 11.

6.2 Bending of a degrading beam

Herein, we shall consider pure bending of a degrading beam. At time $t = 0$, a finite degrading beam is suddenly bent by an action of pure end moments. For $t > 0$, the centerline of the beam becomes a sector of a circle of

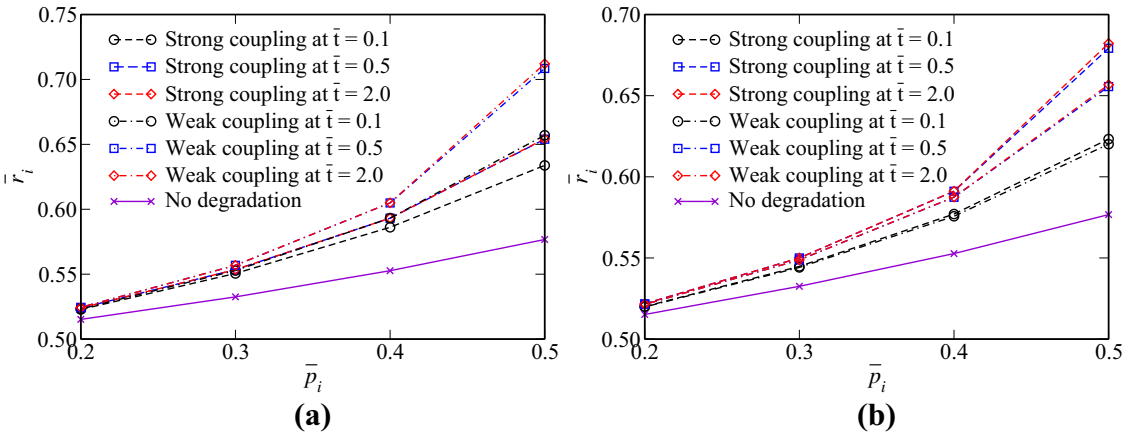

Fig. 9 Inflation of a degrading spherical shell: This figure shows the plot of inner radius $\overline{r}_i$ in current configuration as a function of the inner pressure $\overline{p}_i$ for strongly and weakly coupled chemo–thermo–mechano degradation problem. Note that in weak coupling the heat conductivity and diffusivity are both constants, while the Lamé parameters still depend on concentration and temperature. We take $\overline{\mu}_1 = 0.3$ and $\overline{\mu}_2 = 0.4$ for thermo-dominated degradation. For chemo-dominated degradation, we have $\overline{\mu}_1 = 0.7$ and $\overline{\mu}_2 = 0.1$. For a given $\overline{p}_i$, one can see that $\overline{r}_i$ for weak coupling is larger than strong coupling when thermal degradation dominates. This is because $\overline{I}_{\mathbf{E}}$ is always positive in this problem, the thermal conductivity decreases due to the increase in $\overline{I}_{\mathbf{E}}$. However, when moisture-induced degradation dominates, $\overline{r}_i$ for weak coupling is smaller than strong coupling problem. From this figure, we can observe creep-like behavior for all the case studies. **a** Thermo-dominated degradation, **b** chemo-dominated degradation

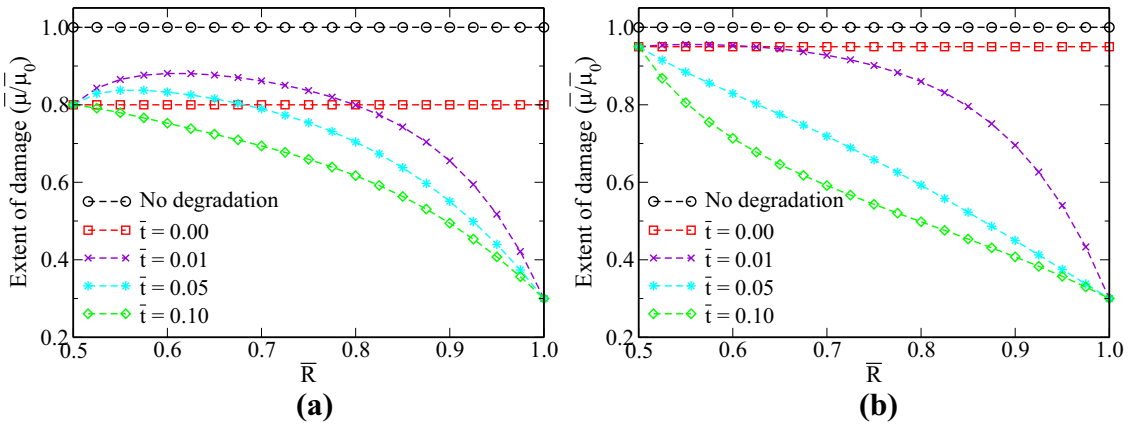

Fig. 10 Inflation of a degrading spherical shell: This figure shows the extent of damage as a function of the reference location at various instants of time due to inner pressure $\overline{p}_i = 0.5$. Different values are chosen for $\overline{\mu}_1$ and $\overline{\mu}_2$ for thermo-dominant and chemo-dominant degradation. Analysis is performed for strongly coupled case. For thermo-dominated problem, healing-like behavior is observed at early time steps. This is because of the deformation-dependent thermal diffusivity. As $\overline{\vartheta} \leq \overline{\vartheta}_0$, the material damage is less than that of at time $\bar{t} = 0$ (but still remains below that of the virgin material). However, this heal-like behavior becomes less distinct (or even does not exist) when the chemo-degradation achieves the dominance. **a** Thermo-dominated degradation, **b** chemo-dominated degradation

radius r_c. This centerline is held fixed for all the time. Subsequently, the stresses in the degrading beam are allowed to relax. In addition, it is assumed that the material remains isotropic with respect to the reference configuration throughout the degradation process. These assumptions enable us to employ the counterpart of universal deformations (also known as semi-inverse method) [56] to study such degrading beams.

A pictorial description of the initial boundary value problem is shown in Fig. 12. The degrading beam is defined as follows:

$$-L \leq X \leq L, \quad -W \leq Y \leq W, \quad -H \leq Z \leq H \tag{6.26}$$

where (X, Y, Z) are the Cartesian coordinates in the reference configuration. We assume that the deformation to be as follows:

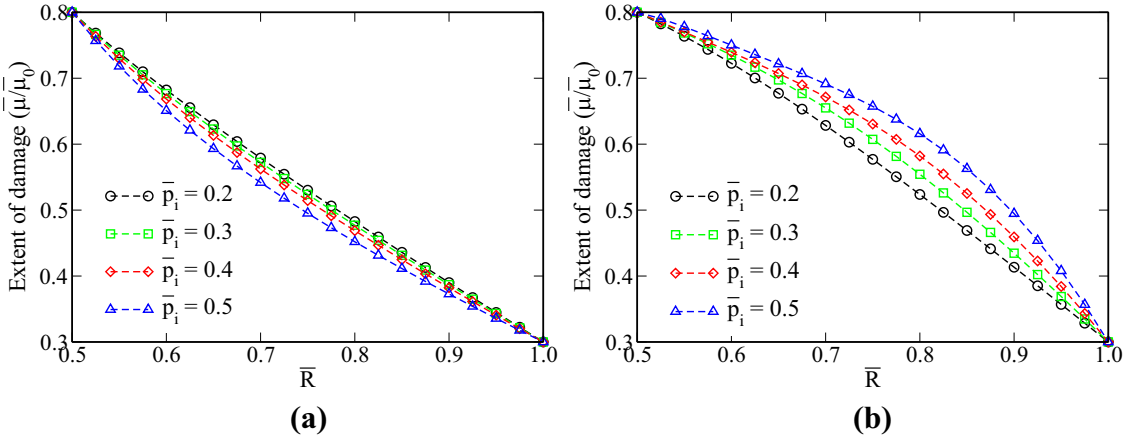

Fig. 11 Inflation of a degrading spherical shell: This figure shows the extent of damage as a function of the reference location at $\bar{t} = 1$ for various inner pressures '$\bar{p}_i$'. Analysis is performed for thermo-dominated degradation. As the pressure increases, for the weakly coupled problem, the extent of damage decreases. This means that when the inflation pressure $\bar{p}_i$ increases, the body degrades more significantly. However, this is not the case for the strongly coupled problem. In this particular case, thermo-mechano coupling dominates and plays a vital role. As $\bar{I}_{\mathbf{E}} \geq 0$, the strain-dependent thermal conductivity decreases as the pressure loading increases. Hence, there is less damage in the material due to the decrease in temperature values as compared to weakly coupled chemo–thermo–mechano degradation problem. **a** Weak coupling degradation, **b** strong coupling degradation

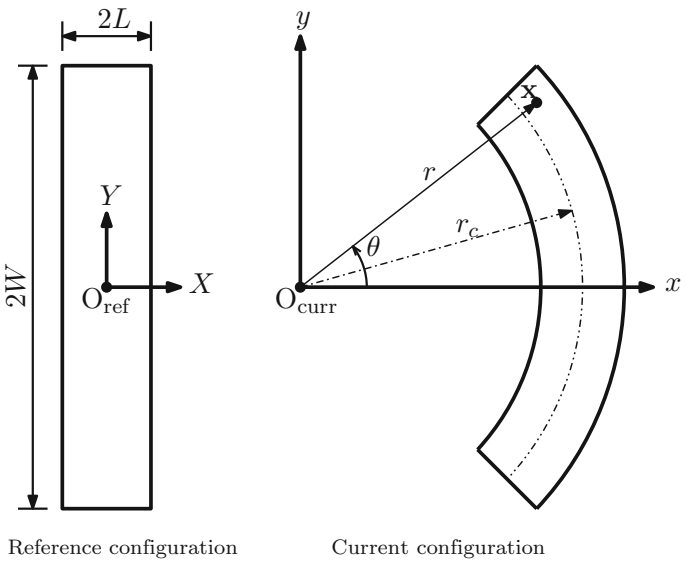

Fig. 12 Bending of a degrading beam: A pictorial description of degrading beam in both reference and current configurations. Bending moment is applied at the two ends of the beam just after time $\bar{t} = 0$. O_{ref} and O_{curr} correspond to the origin in the reference and current configurations

$$r = \sqrt{\frac{2X}{\alpha} + \beta}, \quad \theta = \frac{Y}{\gamma}, \quad z = Z \tag{6.27}$$

where (r, θ, z) are the cylindrical polar coordinates in the current configuration. When $X = 0$, we have $\beta = r_c^2$. It should be noted that α and γ are all unknown time-dependent parameters. These unknowns are evaluated from the incompressibility constraint, traction boundary conditions, and pure end moments. To reduce the complexity in finding semi-analytical solutions, we shall assume r_c is given. The faces $X = -L$ and $X = L$ are subjected to ambient atmospheric pressure "p_{atm}." Upon deformation, the corresponding deformed faces r_i and r_o are maintained at p_{atm}, where $r_i = \sqrt{r_c^2 - 2\gamma L}$ and $r_o = \sqrt{r_c^2 + 2\gamma L}$ are the inner and outer radius of the degrading beam. This gives the following traction boundary conditions:

$$T_{rr}(X = -L, t) = T_{rr}(X = L, t) = p_{\text{atm}} \tag{6.28}$$

The deformation gradient **F**, right Cauchy–Green tensor **C**, and left Cauchy–Green tensor **B** for the degrading beam are given as follows:

$$\{\mathbf{F}\} = \begin{pmatrix} \frac{1}{\alpha r} & 0 & 0 \\ 0 & \frac{r}{\gamma} & 0 \\ 0 & 0 & 1 \end{pmatrix} \qquad \{\mathbf{C}\} = \{\mathbf{B}\} = \begin{pmatrix} \frac{1}{\alpha^2 r^2} & 0 & 0 \\ 0 & \frac{r^2}{\gamma^2} & 0 \\ 0 & 0 & 1 \end{pmatrix} \tag{6.29}$$

For incompressible degrading neo-Hookean material, we have $\alpha\gamma = 1$ and the nonzero components of the Cauchy stress tensor are given as follows:

$$T_{rr} = -p + \frac{\mu(c,\vartheta)\gamma^2}{2\gamma X + r_c^2}, \quad T_{\theta\theta} = -p + \frac{\mu(c,\vartheta)\left(2\gamma X + r_c^2\right)}{\gamma^2}, \quad T_{zz} = -p + \mu(c,\vartheta) \tag{6.30}$$

The balance of linear momentum in the cylindrical polar coordinates reduces to the following:

$$\frac{\partial T_{rr}}{\partial r} + \frac{T_{rr} - T_{\theta\theta}}{r} = 0, \quad \frac{\partial p}{\partial \theta} = 0, \quad \frac{\partial p}{\partial z} = 0 \tag{6.31}$$

The bending moment in the deformation subproblem can be evaluated based on the following formula:

$$\begin{aligned} M_{\text{beam}}(t) &= \int_{A_{\text{cross}}} T_{\theta\theta}(r - r_{\text{neu}})\mathrm{d}A \\ &= 2H \int_{-L}^{L} T_{\theta\theta}(-\sqrt{r_c^2 + 2\gamma X_{\text{neu}}} + \sqrt{r_c^2 + 2\gamma X})\frac{\gamma}{\sqrt{r_c^2 + 2\gamma X}}\mathrm{d}X \end{aligned} \tag{6.32}$$

where $\mathrm{d}A = 2H\mathrm{d}r$, $r_{\text{neu}} = \sqrt{r_c^2 + 2\gamma X_{\text{neu}}}$ is the neutral axis location, and X_{neu} is the value at which $T_{\theta\theta} = 0$. The chemical potential, specific entropy for the degrading beam are given as follows:

$$\varkappa = \frac{1}{\rho_0}\frac{\partial \psi}{\partial c} + R_s\vartheta_{\text{ref}}\{c - c_{\text{ref}}\} = -\frac{\mu_1}{2\rho_0 c_{\text{ref}}}\left(\frac{\gamma^2}{r^2} + \frac{r^2}{\gamma^2} - 2\right) + R_s\vartheta_{\text{ref}}\{c - c_{\text{ref}}\} \tag{6.33a}$$

$$\eta = -\frac{1}{\rho_0}\frac{\partial \psi}{\partial \vartheta} + \frac{c_p}{\vartheta_{\text{ref}}}\{\vartheta - \vartheta_{\text{ref}}\} = \frac{\mu_1}{2\rho_0\vartheta_{\text{ref}}}\left(\frac{\gamma^2}{r^2} + \frac{r^2}{\gamma^2} - 2\right) + \frac{c_p}{\vartheta_{\text{ref}}}\{\vartheta - \vartheta_{\text{ref}}\} \tag{6.33b}$$

Most of the non-dimensional quantities are same as that of the degrading shell problem except for the following:

$$\overline{r} = \frac{r}{r_c}, \ \overline{X} = \frac{X}{r_c}, \ \overline{\gamma} = \frac{\gamma}{r_c}, \ \overline{t} = \frac{D_0 t}{r_c^2} \tag{6.34}$$

Using Eqs. (6.27)–(6.31), we have the following nonlinear equation in $\overline{\gamma}$

$$\int_{-L/r_c}^{L/r_c} \frac{\overline{\mu}(\overline{c}(\overline{X},\overline{t}),\overline{\vartheta}(\overline{X},\overline{t}))\left(\overline{\gamma}^4 - \left(2\overline{\gamma}\overline{X} + 1\right)^2\right)}{\overline{\gamma}\left(2\overline{\gamma}\overline{X} + 1\right)^2}\mathrm{d}\overline{X} = 0 \tag{6.35}$$

From (6.35), $\overline{\gamma}|_{\overline{t}=0}$ is given as follows:

$$\overline{\gamma}|_{\overline{t}=0} = \frac{1}{r_c}\sqrt{-2L^2 + \sqrt{4L^4 + r_c^4}} \tag{6.36}$$

which is the case for homogeneous neo-Hookean material. As r_c is given, the parameter $\overline{\gamma}$ is bounded above and below as follows:

$$\frac{-r_c}{2L} < \overline{\gamma} < \frac{r_c}{2L} \tag{6.37}$$

which can be used in finding the solution for the nonlinear equation given by (6.35). It should be noted that $\overline{\gamma}|_{t=0}$ satisfies the inequality given by (6.37).

From Eqs. (6.1) and (6.2), the final form for the governing equations for transport and thermal subproblems for degrading beam is given as follows:

$$\frac{\partial \overline{c}}{\partial \overline{t}} - \left(\frac{\overline{D}_{\varkappa\varkappa}}{\overline{r}} + \frac{\partial \overline{D}_{\varkappa\varkappa}}{\partial \overline{r}}\right)\frac{\partial \overline{c}}{\partial \overline{r}} - \overline{D}_{\varkappa\varkappa}\frac{\partial^2 \overline{c}}{\partial \overline{r}^2} = \overline{\omega}\frac{\partial \overline{D}_{\varkappa\varkappa}}{\partial \overline{r}}\left(\frac{\overline{\gamma}^2}{\overline{r}^3} - \frac{\overline{r}}{\overline{\gamma}^2}\right) - 2\overline{\omega}\overline{D}_{\varkappa\varkappa}\left(\frac{1}{\overline{\gamma}^2} + \frac{\overline{\gamma}^2}{\overline{r}^4}\right) \tag{6.38}$$

$$\overline{\vartheta}\frac{\partial \overline{\vartheta}}{\partial \overline{t}} - \left(\frac{\overline{D}_{\vartheta\vartheta}}{\overline{r}} + \frac{\partial \overline{D}_{\vartheta\vartheta}}{\partial \overline{r}}\right)\frac{\partial \overline{\vartheta}}{\partial \overline{r}} - \overline{D}_{\vartheta\vartheta}\frac{\partial^2 \overline{\vartheta}}{\partial \overline{r}^2} = \overline{\tau}\overline{D}_{\varkappa\varkappa}\left(\frac{\partial \overline{c}}{\partial \overline{r}} + \overline{\omega}\left(\frac{\overline{\gamma}^2}{\overline{r}^3} - \frac{\overline{r}}{\overline{\gamma}^2}\right)\right)^2 \tag{6.39}$$

6.2.1 Steady-state and unsteady analysis for beam degradation

In case of steady state, we have $h_r r = C_1$ and $q_r r + \varkappa h_r r = C_2$, where C_1 and C_2 are integration constants. Equations (6.38) and (6.39) imply that $\overline{c}$ and $\overline{\vartheta}$ are the solutions of the following ODEs:

$$\overline{D}_{\varkappa\varkappa}\overline{r}\frac{\mathrm{d}\overline{c}}{\mathrm{d}\overline{r}} - \overline{D}_{\varkappa\varkappa}\overline{\omega}\left(\frac{\overline{\gamma}^2}{\overline{r}^2} - \frac{\overline{r}^2}{\overline{\gamma}^2}\right) + \overline{C}_1 = 0 \tag{6.40a}$$

$$\overline{D}_{\vartheta\vartheta}\overline{r}\frac{\mathrm{d}\overline{\vartheta}}{\mathrm{d}\overline{r}} + \overline{\tau}\left(\frac{\overline{w}}{2}\left(\frac{\overline{\gamma}^2}{\overline{r}^2} + \frac{\overline{r}^2}{\overline{\gamma}^2} - 2\right) - \overline{c} + 1\right)\overline{C}_1 + \overline{C}_2 = 0 \tag{6.40b}$$

In case of weak coupling (where $D_{\vartheta\vartheta}$ and $D_{\varkappa\varkappa}$ are constants), the solutions for $\overline{c}$ and $\overline{\vartheta}$ take the following simplified form:

$$\overline{c} = -\frac{\overline{\omega}}{2}\left(\frac{\overline{\gamma}^2}{\overline{r}^2} + \frac{\overline{r}^2}{\overline{\gamma}^2}\right) + B_2\ln[\overline{r}] + A_2, \quad \overline{\vartheta} = -\frac{\overline{\tau}B_2^2\overline{D}_{\varkappa\varkappa}}{2\overline{D}_{\vartheta\vartheta}}\ln[\overline{r}]^2 + Z_2\ln[\overline{r}] + Y_2 \tag{6.41}$$

where the constants A_2, B_2, Y_2, and Z_2 (which depend on the boundary conditions) are as follows:

$$A_2 = \overline{c}_i - B_2\ln[\overline{r}_i] + \frac{\overline{\omega}}{2}\left(\frac{\overline{\gamma}^2}{\overline{r}_i^2} + \frac{\overline{r}_i^2}{\overline{\gamma}^2}\right) \tag{6.42a}$$

$$B_2 = \frac{1}{\ln[\overline{r}_o] - \ln[\overline{r}_i]}\left(\overline{c}_o - \overline{c}_i - \frac{\overline{\omega}}{2}\left(\frac{\overline{\gamma}^2}{\overline{r}_i^2} + \frac{\overline{r}_i^2}{\overline{\gamma}^2} - \frac{\overline{\gamma}^2}{\overline{r}_o^2} - \frac{\overline{r}_o^2}{\overline{\gamma}^2}\right)\right) \tag{6.42b}$$

$$Y_2 = \overline{\vartheta}_i + \frac{\overline{\tau}B_2^2\overline{D}_{\varkappa\varkappa}}{2\overline{D}_{\vartheta\vartheta}}\ln[\overline{r}_i]^2 - Z_2\ln[\overline{r}_i] \tag{6.42c}$$

$$Z_2 = \frac{1}{\ln[\overline{r}_o] - \ln[\overline{r}_i]}\left(\overline{\vartheta}_o - \overline{\vartheta}_i - \frac{\overline{\tau}B_2^2\overline{D}_{\varkappa\varkappa}}{2\overline{D}_{\vartheta\vartheta}}\left(\ln[\overline{r}_i]^2 - \ln[\overline{r}_o]^2\right)\right) \tag{6.42d}$$

For unsteady analysis, we employ method of horizontal lines with backward Euler time-stepping scheme. This gives the following ODEs at each time level for Eqs. (6.38) and (6.39):

$$\begin{aligned}\frac{\mathrm{d}^2\overline{c}^{(n+1)}}{\mathrm{d}\overline{r}^2} + \left(\frac{1}{\overline{r}^{(n)}} + \left(\frac{1}{\overline{D}_{\varkappa\varkappa}^{(n)}}\right)\frac{\mathrm{d}\overline{D}_{\varkappa\varkappa}}{\mathrm{d}\overline{r}}\bigg|_{\overline{t}=\overline{t}_n}\right)\frac{\mathrm{d}\overline{c}^{(n+1)}}{\mathrm{d}\overline{r}} - \frac{\overline{c}^{(n+1)}}{\overline{D}_{\varkappa\varkappa}^{(n)}\Delta\overline{t}} &= 2\overline{\omega}\left(\frac{1}{\left(\overline{\gamma}^{(n)}\right)^2} + \frac{\left(\overline{\gamma}^{(n)}\right)^2}{\left(\overline{r}^{(n)}\right)^4}\right) \\ - \frac{\overline{c}^{(n)}}{\overline{D}_{\varkappa\varkappa}^{(n)}\Delta\overline{t}} - \left(\frac{\overline{\omega}}{\overline{D}_{\varkappa\varkappa}^{(n)}}\right)\left(\frac{\mathrm{d}\overline{D}_{\varkappa\varkappa}}{\mathrm{d}\overline{r}}\bigg|_{\overline{t}=\overline{t}_n}\right)&\left(\frac{\left(\overline{\gamma}^{(n)}\right)^2}{\left(\overline{r}^{(n)}\right)^3} - \frac{\overline{r}^{(n)}}{\left(\overline{\gamma}^{(n)}\right)^2}\right)\end{aligned} \tag{6.43}$$

$$\frac{\mathrm{d}^2\overline{\vartheta}^{(n+1)}}{\mathrm{d}\overline{r}^2} + \left(\frac{1}{\overline{r}^{(n)}} + \left(\frac{1}{\overline{D}_{\vartheta\vartheta}^{(n)}}\right)\frac{\mathrm{d}\overline{D}_{\vartheta\vartheta}}{\mathrm{d}\overline{r}}\bigg|_{\overline{t}=\overline{t}_n}\right)\frac{\mathrm{d}\overline{\vartheta}^{(n+1)}}{\mathrm{d}\overline{r}} - \frac{\overline{\vartheta}^{(n)}\overline{\vartheta}^{(n+1)}}{\overline{D}_{\vartheta\vartheta}^{(n)}\Delta\overline{t}} = -\frac{\overline{\tau}\overline{D}_{\varkappa\varkappa}^{(n)}}{\overline{D}_{\vartheta\vartheta}^{(n)}}\left(\frac{\mathrm{d}\overline{c}}{\mathrm{d}\overline{r}}\bigg|_{\overline{t}=\overline{t}_n}\right)^2 - \frac{\left(\overline{\vartheta}^{(n)}\right)^2}{\overline{D}_{\vartheta\vartheta}^{(n)}\Delta\overline{t}}$$

$$-\frac{2\overline{\tau}\overline{\omega}\overline{D}^{(n)}_{\varkappa\varkappa}}{\overline{D}^{(n)}_{\vartheta\vartheta}}\left(\frac{\left(\overline{\gamma}^{(n)}\right)^2}{\left(\overline{r}^{(n)}\right)^3}-\frac{\overline{r}^{(n)}}{\left(\overline{\gamma}^{(n)}\right)^2}\right)\frac{\mathrm{d}\overline{c}}{\mathrm{d}\overline{r}}\bigg|_{\overline{t}=\overline{t}_n}-\frac{\overline{\tau}\overline{D}^{(n)}_{\varkappa\varkappa}\overline{\omega}^2}{\overline{D}^{(n)}_{\vartheta\vartheta}}\left(\frac{\left(\overline{\gamma}^{(n)}\right)^2}{\left(\overline{r}^{(n)}\right)^3}-\frac{\left(\overline{r}^{(n)}\right)}{\left(\overline{\gamma}^{(n)}\right)^2}\right)^2 \tag{6.44}$$

Algorithm 2 describes a procedure to determine $\overline{c}(\overline{r},\overline{t})$, $\overline{\vartheta}(\overline{r},\overline{t})$, and $\overline{\gamma}$ at various times using an iterative nonlinear numerical solution strategy. The boundary conditions for diffusion and thermal subproblems are the same as the degrading shell problem. The other parameters are assumed in the strongly coupling simulations as follows:

$$\begin{aligned}&\overline{L}=1,\ \overline{r}_c=1,\ \Delta\overline{t}=0.1,\ \overline{t}=2,\ \overline{\omega}=0.05,\ \overline{\tau}=0.5,\ \overline{\mu}_0=1,\ \overline{\mu}_1=\overline{\mu}_2=0.4,\ \overline{D}_0=1,\\&\overline{D}_T=2.0,\ \overline{D}_S=1.5,\ \eta_T=\eta_S=1,\ E_{\mathrm{ref}T}=E_{\mathrm{ref}S}=1,\ \overline{K}_0=1,\ \delta=10\end{aligned} \tag{6.45}$$

In case of weak coupling, we have $\overline{D}_0$ as $\overline{D}^{(n)}_{\varkappa\varkappa}$ and $\overline{K}_0$ as $\overline{D}^{(n)}_{\vartheta\vartheta}$, respectively.

Algorithm 2 Pure bending of degrading beam (numerical methodology to find $\overline{\gamma}$, $\overline{c}$, and $\overline{\vartheta}$)

1: INPUT: Non-dimensional material parameters, non-dimensional boundary conditions, and non-dimensional initial conditions, `MaxIters` (which is taken to be equal to 100), tolerances $\epsilon^{(\gamma)}_{\mathrm{tol}}$, $\epsilon^{(c)}_{\mathrm{tol}}$, and $\epsilon^{(\vartheta)}_{\mathrm{tol}}$.
2: Evaluate $\overline{\gamma}$ at $\overline{t}=0$ based on Eq. (6.36). Use this as an initial guess for solving nonlinear equation given by (6.35) or guess $\overline{\gamma}$ based on Eq. (6.37).
3: **for** $n=1,2,\ldots,N$ **do**
4: **for** $i=1,2,\ldots$ **do**
5: **if** $i >$ `MaxIters` **then**
6: Solution did not converge in specified maximum number of iterations. EXIT.
7: **end if**
8: `Diffusion subproblem`: Given $\overline{\gamma}^{(i)}$, solve Eq. (6.43) to obtain $\overline{c}^{(i+1)}$. Herein, we use shooting method to solve the ODEs.
9: `Heat conduction subproblem`: Given $\overline{\gamma}^{(i)}$ and $\overline{c}^{(i+1)}$, solve Eq. (6.44) to obtain $\overline{\vartheta}^{(i+1)}$. Similarly, we use shooting method to solve the ODEs.
10: `Deformation subproblem`: Given $\overline{c}^{(i+1)}$ and $\overline{\vartheta}^{(i+1)}$, solve for $\overline{\gamma}^{(i+1)}$ given by Eq. (6.35) using bisection method.
11: **if** $\|\overline{\gamma}^{(i+1)}-\overline{\gamma}^{(i)}\|<\epsilon^{(\gamma)}_{\mathrm{tol}}$, $\|\overline{c}^{(i+1)}-\overline{c}^{(i)}\|<\epsilon^{(c)}_{\mathrm{tol}}$, and $\|\overline{\vartheta}^{(i+1)}-\overline{\vartheta}^{(i)}\|<\epsilon^{(\vartheta)}_{\mathrm{tol}}$ **then**
12: OUTPUT: $\overline{\gamma}^{(i+1)}$, $\overline{c}^{(i+1)}$, and $\overline{\vartheta}^{(i+1)}$. EXIT the inner loop.
13: **else**
14: Update the guess: $\overline{\gamma}^{(i)}\leftarrow\overline{\gamma}^{(i+1)}$.
15: **end if**
16: **end for**
17: **end for**

The numerical results are shown in Figs. 13, 14, 15 and 16, which reveal the following conclusions on the overall behavior of bending of degrading beams:

1. Degradation versus non-degradation: *The main observation is that the neutral axis shifts further to the left in Fig. 13, similar to the phenomenon observed in viscoelastic solids [42].* Moreover, in case of weak coupling for some instants of time *the maximum stress does not occur at either tensile or compressive sides of the beam after the onset of degradation*. This is of primal importance in regard to the calculation of failure loads/moments due to material damage. Hence, a simple approach based on strength of materials or a more complex finite elasticity theory to calculate stresses without accounting for degradation will lead to erroneous results.
2. Initially at $\overline{t}=0$ and when there is no degradation, the response is that of a homogeneous neo-Hookean material, see Fig. 16. *On the onset of degradation, the material ceases to be homogeneous.*
3. In Fig. 14, moment relaxation is observed for weak and strong coupling degradation. Note that the moment is a constant without degradation. Moreover, although diffusion is dominant in the coupling effect for chemical potential, one can still observe the deformation effect on $\overline{\varkappa}$ as compared to no degradation case in Fig. 15.
4. Strong versus weak coupling: One can see that $\overline{T}_{\theta\theta}$ for strong coupling is considerably different from the weak coupling in Fig. 13. This is because the degradation progress is dependent on the deformation, concentration of the diffusing chemical species, and temperature of the body.
5. In Fig. 16, the extent of damage is monotonic for weak coupling, which is not the case for strong coupling (which helps in identifying regions that need retrofitting).

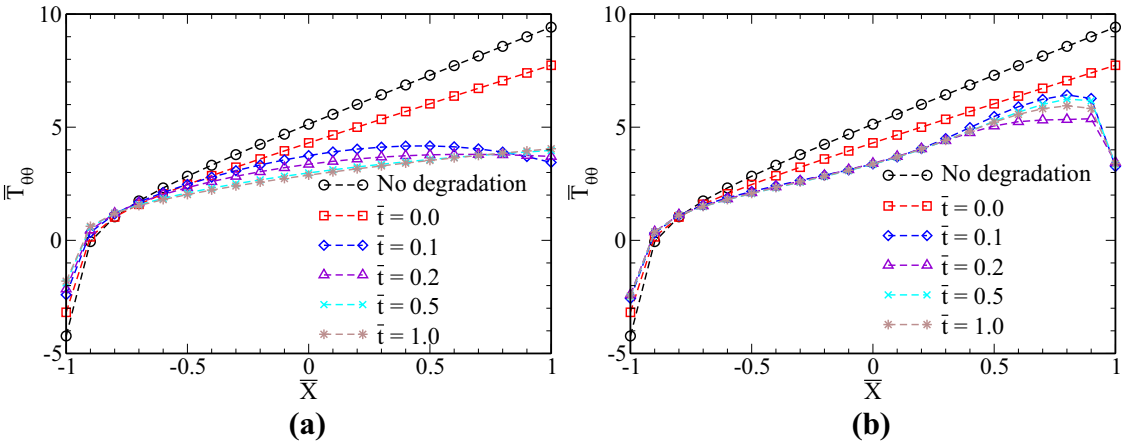

Fig. 13 Bending of a degrading beam: This figure shows the plot of hoop stress $\overline{T}_{\theta\theta}$ as a function of the reference location of the cross section at various instants of time. The stress distribution is not linear, which is the case for finite deformation beam bending problem. Herein, we observe that the neutral axis shifts further to the left. Moreover, in case of weak coupling for some instants of time the maximum stress does not occur at either tensile or compressive sides of the beam after the onset of degradation. **a** Weak coupling degradation, **b** strong coupling degradation

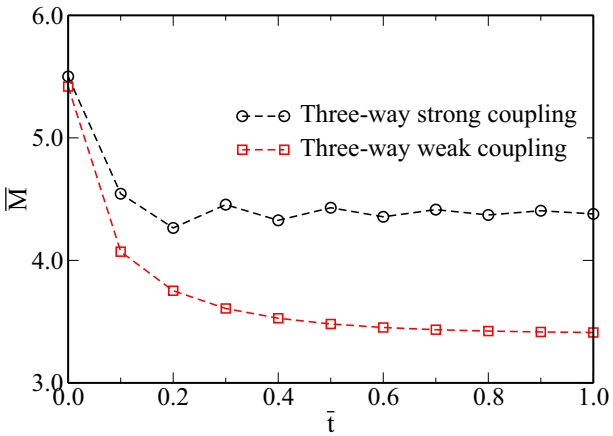

Fig. 14 Bending of a degrading beam: This figure shows the plot of bending moment at various instants of time for both strong and weak coupling chemo–thermo–mechano degradation. Moment relaxation is observed for both cases; however, in weak coupling the moment declines at a much faster rate than that in strong coupling case. Note that the bending moment is a constant without degradation

Remark 6.1 It should be mentioned that [63] have shown that the neutral axis shifts under pure bending of a polymer beam under mechanical degradation. However, their approach is based on internal variables and by employing a semi-inverse method. Herein, we have illustrated a similar behavior of a degrading beam using the proposed chemo–thermo–mechanical framework, which considers various coupled processes, as opposed to a lumped internal variable approach.

6.3 Torsional shear of a degrading cylinder

A pictorial description of the degrading cylindrical annulus of finite length is shown in Fig. 17. The bottom of the cylinder is fixed and just after time $t = 0$, a twisting moment is applied. We analyze the material degradation and corresponding structural response due to the torsional shear for a prescribed angle of twist. Initially, the body is a homogeneous neo-Hookean material and there is no transport of chemical species in the body. For time $t > 0$, the outer boundary of the cylinder is always exposed to moisture (or a diffusing chemical species). The inner surface of the degrading annular cylinder is held at zero concentration. This can be achieved by constructing a mechanism which continuously removes the moisture (or diffusing chemical

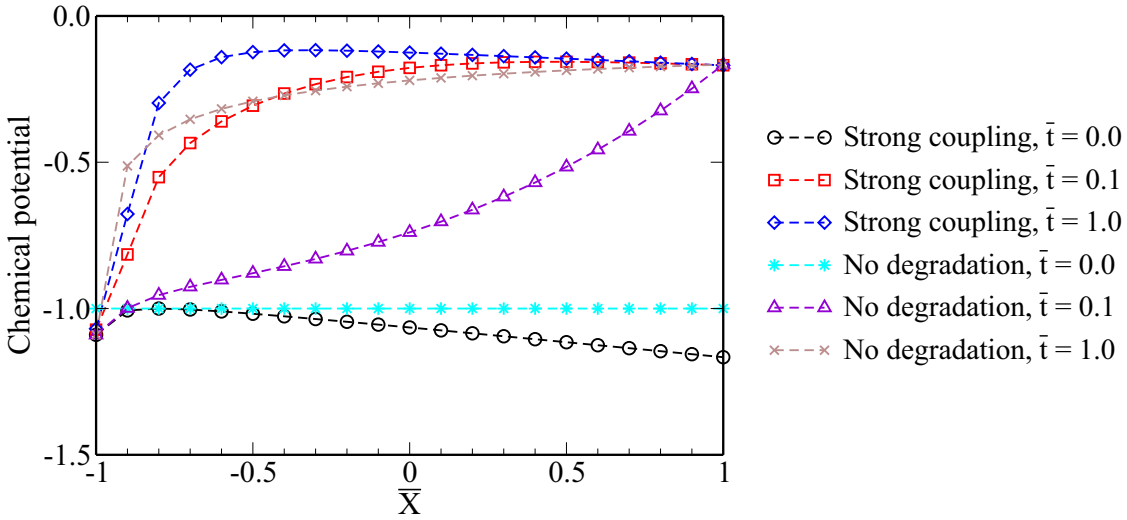

Fig. 15 Bending of a degrading beam: This figure shows the plot of chemical potential as a function of the reference location of the cross section at various instants of time when there is no degradation and for strong coupling cases. In the strong coupling scenario, although diffusion process is dominant, one can still observe that the deformation has a significant effect on chemical potential as compared with non-degradation case

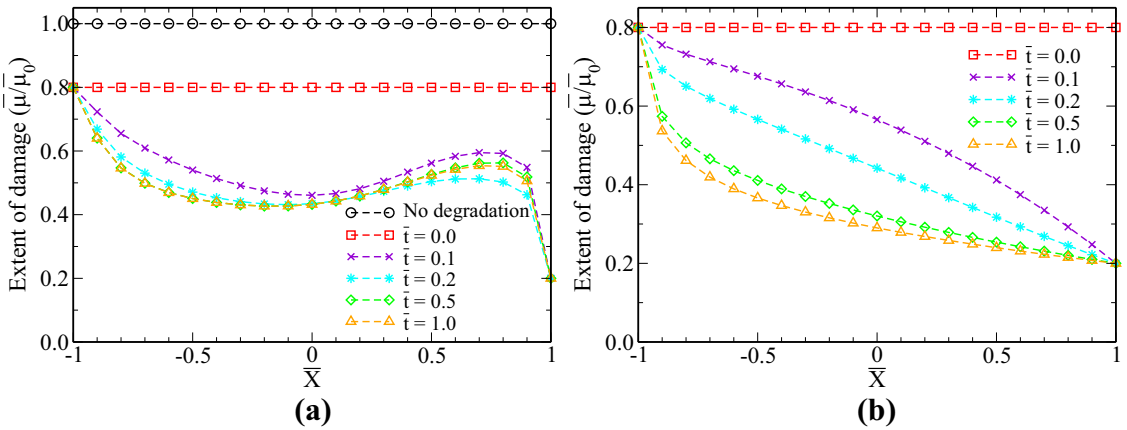

Fig. 16 Bending of a degrading beam: This figure shows the extent of damage as a function of the reference location of the cross section at various instants of time (due to the application of bending moment). Note that analysis is performed for both strongly coupled and weakly coupled chemo–thermo–mechano degradation. One can see that *a virgin beam, which is initially homogeneous, is no longer homogeneous after degradation*. In addition, the extent of damage is monotonic for weak coupling, which is not the case for strong coupling. Such a phenomena has implications in damage control and retrofitting of the degrading beams. **a** Strong coupling degradation, **b** weak coupling degradation

species) from the inner boundary of the degrading cylinder. Hence, one can control the concentration of the moisture at both inner and outer surfaces. Similar type of initial and boundary conditions is enforced for the thermal counterpart.

Consider a closed cylindrical body of inner radius R_i, outer radius R_o, and height L defined as follows:

$$R_i \leq R \leq R_o, \quad 0 \leq \Theta \leq 2\pi, \quad 0 \leq Z \leq L \tag{6.46}$$

where (R, Θ, Z) are the cylindrical polar coordinates in the reference configuration. Under torsional shear, the deformation can be described as follows:

$$r = R, \quad \theta = \Theta + g(Z, t), \quad z = \Lambda Z \tag{6.47}$$

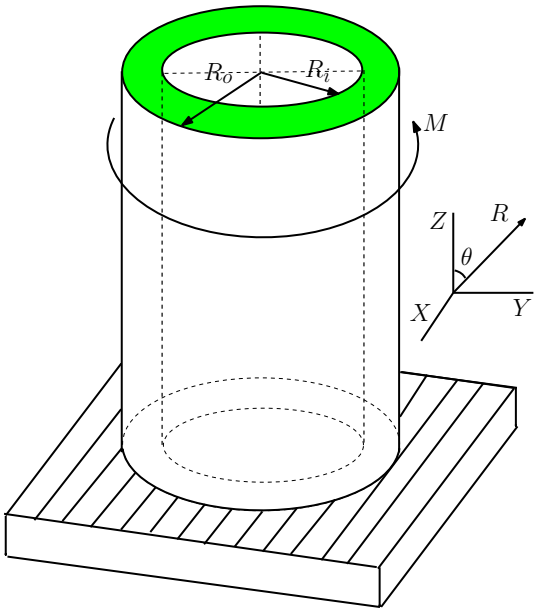

Fig. 17 Torsional shear of a degrading cylinder: A pictorial description of the degrading cylinder under torsion in the reference configuration. R_i and R_o are, respectively, the inner and outer radii of the cylinder. X, Y, and Z are the Cartesian coordinates in the reference configuration. The bottom of the cylinder is fixed and a twisting moment is applied at the top of the cylinder for $t \geq 0$

The components of the deformation gradient **F** can be written as:

$$\{\mathbf{F}\} = \begin{pmatrix} 1 & 0 & 0 \\ 0 & 1 & rg' \\ 0 & 0 & \Lambda \end{pmatrix} \quad \text{where } g' := \frac{\partial g(Z,t)}{\partial Z} \tag{6.48}$$

Incompressibility implied that $\Lambda = 1$. The components of the right Cauchy–Green tensor **C** and the left Cauchy–Green tensor **B** can be written as:

$$\{\mathbf{C}\} = \begin{pmatrix} 1 & 0 & 0 \\ 0 & 1 & rg' \\ 0 & rg' & 1 + \left(rg'\right)^2 \end{pmatrix} \quad \{\mathbf{B}\} = \begin{pmatrix} 1 & 0 & 0 \\ 0 & 1 + \left(rg'\right)^2 & rg' \\ 0 & rg' & 1 \end{pmatrix} \tag{6.49}$$

The nonzero components of the Cauchy stress **T** are given as follows:

$$\begin{aligned} T_{rr} &= -p + \mu(c,\vartheta), \quad T_{\theta\theta} = -p + \mu(c,\vartheta)\left(1 + \left(rg'\right)^2\right) \\ T_{zz} &= -p + \mu(c,\vartheta), \quad T_{\theta z} = T_{z\theta} = \mu(c,\vartheta) rg' \end{aligned} \tag{6.50}$$

The balance of linear momentum in the cylindrical polar coordinates reduces to the following:

$$-\frac{\partial p}{\partial r} + \mu(c,\vartheta) r \left(g'\right)^2 = 0, \quad -\frac{1}{r}\frac{\partial p}{\partial \theta} + \mu(c,\vartheta) rg'' = 0, \quad -\frac{\partial p}{\partial z} = 0 \tag{6.51}$$

Symmetry in the problem implies that $\frac{\partial p}{\partial \theta} = 0$, which further implies that $g'' = 0$. Hence, $g(Z,t)$ takes the following form:

$$g(Z,t) = \Psi_1(t) Z + \Psi_2(t) \tag{6.52}$$

where Ψ_1 and Ψ_2 are evaluated based on the input data. As the bottom of the cylinder is fixed, we have $g(Z=0,t) = 0$, which implies $\Psi_2(t) = 0$.

The chemical potential and specific entropy are given as follows:

$$\varkappa = \frac{1}{\rho_0}\frac{\partial \psi}{\partial c} + R_s \vartheta_{\text{ref}}\{c - c_{\text{ref}}\} = -\frac{\mu_1 r^2 \Psi_1^2}{2\rho_0 c_{\text{ref}}} + R_s \vartheta_{\text{ref}}\{c - c_{\text{ref}}\} \tag{6.53a}$$

$$\eta = -\frac{1}{\rho_0}\frac{\partial \psi}{\partial \vartheta} + \frac{c_p}{\vartheta_{\text{ref}}}\{\vartheta - \vartheta_{\text{ref}}\} = \frac{\mu_1 r^2 \Psi_1^2}{2\rho_0 \vartheta_{\text{ref}}} + \frac{c_p}{\vartheta_{\text{ref}}}\{\vartheta - \vartheta_{\text{ref}}\} \tag{6.53b}$$

Most of the non-dimensional quantities remain the same as that of the previous initial boundary value problems except for the following:

$$\overline{R} = \frac{R}{R_o},\ \overline{\psi} = \psi R_o,\ \bar{t} = \frac{D_0 t}{R_o^2} \tag{6.54}$$

The non-dimensional twisting moment $\overline{M}(\bar{t})$ satisfies:

$$\overline{M}(\bar{t}) = 2\pi \int_{\overline{R}_i}^{\overline{R}_o} \overline{\mu}(\overline{c}(\overline{R}, \bar{t}), \overline{\vartheta}(\overline{R}, \bar{t}))\overline{\Psi}_1 \overline{R}^3 \mathrm{d}\overline{R} \tag{6.55}$$

The Poynting effect for hyperelastic materials shall be also studied. It implies the axial length change for a cylinder under shear. The non-dimensional normal force required to keep the length unchanged can be written as follows:

$$\overline{N}(\bar{t}) = \pi \int_{\overline{R}_i}^{\overline{R}_o} \overline{\mu}(\overline{c}(\overline{R}, \bar{t}), \overline{\vartheta}(\overline{R}, \bar{t}))\overline{\Psi}_1^2 \overline{R}^3 \mathrm{d}\overline{R} \tag{6.56}$$

From Eqs. (6.1) and (6.2), the final form of the governing equations for transport and thermal subproblems can be written as:

$$\frac{\partial \overline{c}}{\partial \bar{t}} - \left(\frac{\overline{D}_{\varkappa\varkappa}}{\bar{r}} + \frac{\partial \overline{D}_{\varkappa\varkappa}}{\partial \bar{r}}\right)\frac{\partial \overline{c}}{\partial \bar{r}} - \overline{D}_{\varkappa\varkappa}\frac{\partial^2 \overline{c}}{\partial \bar{r}^2} = -\overline{\omega}\overline{\Psi}_1^2\left(2\overline{D}_{\varkappa\varkappa} + \bar{r}\frac{\partial \overline{D}_{\varkappa\varkappa}}{\partial \bar{r}}\right) \tag{6.57}$$

$$\overline{\vartheta}\frac{\partial \overline{\vartheta}}{\partial \bar{t}} - \left(\frac{\overline{D}_{\vartheta\vartheta}}{\bar{r}} + \frac{\partial \overline{D}_{\vartheta\vartheta}}{\partial \bar{r}}\right)\frac{\partial \overline{\vartheta}}{\partial \bar{r}} - \overline{D}_{\vartheta\vartheta}\frac{\partial^2 \overline{\vartheta}}{\partial \bar{r}^2} = \overline{\tau}\overline{D}_{\varkappa\varkappa}\left(\frac{\partial \overline{c}}{\partial \bar{r}}\right)^2 - 2\overline{\tau}\overline{\omega}\overline{D}_{\varkappa\varkappa}\bar{r}\overline{\Psi}_1^2\frac{\partial \overline{c}}{\partial \bar{r}} + \overline{\tau}\overline{D}_{\varkappa\varkappa}\overline{\omega}^2\bar{r}^2\overline{\Psi}_1^4 \tag{6.58}$$

One needs to solve Eqs. (6.56)–(6.58) to obtain $\overline{c}(\bar{r}, \bar{t})$, $\overline{\vartheta}(\bar{r}, \bar{t})$, and $\overline{M}(\bar{t})$. Algorithm 3 describes a numerical solution procedure to solve these equations at various times for a given angle of twist per unit length.

Algorithm 3 Torsional shear of a degrading cylinder (numerical methodology to find $\overline{M}$, $\overline{c}$, and $\overline{\vartheta}$)

1: INPUT: Non-dimensional material parameters, non-dimensional boundary conditions, and non-dimensional initial conditions.
2: **for** $n = 1, 2, \ldots, N$ **do**
3: `Diffusion subproblem`: Given $\overline{\Psi}_1$, solve Eq. (6.62) to obtain $\overline{c}^{(n)}$. Herein, we use shooting method to solve the ODEs.
4: `Heat conduction subproblem`: Given $\overline{\Psi}_1$ and $\overline{c}^{(n)}$, solve Eq. (6.63) to obtain $\overline{\vartheta}^{(n)}$. Similar to diffusion subproblem, we use shooting method to solve the nonlinear ODEs.
5: `Deformation subproblem`: Given $\overline{c}^{(n)}$ and $\overline{\vartheta}^{(n)}$, solve for $\overline{M}^{(n)}$ given by Eq. (6.56).
6: **end for**

6.3.1 Steady-state and unsteady response of degrading cylinder under torsional shear

In the case of steady state, $\overline{c}$ and $\overline{\vartheta}$ are the solutions of the following ODEs:

$$\overline{D}_{\varkappa\varkappa}\overline{r}^2\frac{\mathrm{d}\overline{c}}{\mathrm{d}\overline{r}} - \overline{D}_{\varkappa\varkappa}\overline{\omega}\overline{r}\overline{\Psi}_1^2 + \overline{C}_1 = 0 \tag{6.59a}$$

$$\overline{D}_{\vartheta\vartheta}\overline{r}\frac{\mathrm{d}\overline{\vartheta}}{\mathrm{d}\overline{r}} + \overline{\tau}\left(\frac{\overline{\omega}}{2}\overline{r}^2\overline{\Psi}_1^2 - \overline{c} + 1\right)\overline{C}_1 + \overline{C}_2 = 0 \tag{6.59b}$$

where $\overline{C}_1$ and $\overline{C}_2$ are integration constants. Under weak coupling (where $D_{\vartheta\vartheta}$ and $D_{\varkappa\varkappa}$ are constants), a simplified form of the analytical solutions for $\overline{c}$ and $\overline{\vartheta}$ is given as follows:

$$\overline{c} = \frac{\overline{\omega}}{2}\overline{r}^2\overline{\Psi}_1^2 + B_3\ln[\overline{r}] + A_3, \quad \overline{\vartheta} = -\frac{\overline{\tau}B_3^2\overline{D}_{\varkappa\varkappa}}{2\overline{D}_{\vartheta\vartheta}}\ln[\overline{r}]^2 + Z_3\ln[\overline{r}] + Y_3 \tag{6.60}$$

where A_3, B_3, Y_3, and Z_3 are constants, which are obtained by the corresponding boundary conditions for thermal and diffusion subproblem. These are given as follows:

$$A_3 = \overline{c}_i - B_3\ln[\overline{r}_i] - \frac{\overline{\omega}}{2}\overline{r}_i^2\overline{\Psi}_1^2 \tag{6.61a}$$

$$B_3 = \frac{1}{\ln[\overline{r}_o] - \ln[\overline{r}_i]}\left(\overline{c}_o - \overline{c}_i - \frac{\overline{\omega}}{2}\left(\overline{r}_o^2\overline{\Psi}_1^2 - \overline{r}_i^2\overline{\Psi}_1^2\right)\right) \tag{6.61b}$$

$$Y_3 = \overline{\vartheta}_i + \frac{\overline{\tau}B_3^2\overline{D}_{\varkappa\varkappa}}{2\overline{D}_{\vartheta\vartheta}}\ln[\overline{r}_i]^2 - Z_3\ln[\overline{r}_i] \tag{6.61c}$$

$$Z_3 = \frac{1}{\ln[\overline{r}_o] - \ln[\overline{r}_i]}\left(\overline{\vartheta}_o - \overline{\vartheta}_i - \frac{\overline{\tau}B_3^2\overline{D}_{\varkappa\varkappa}}{2\overline{D}_{\vartheta\vartheta}}\left(\ln[\overline{r}_i]^2 - \ln[\overline{r}_o]^2\right)\right) \tag{6.61d}$$

For unsteady analysis, method of horizontal lines with backward Euler time-stepping scheme is employed. This gives the following ODEs at each time level:

$$\begin{aligned}\frac{\mathrm{d}^2\overline{c}^{(n+1)}}{\mathrm{d}\overline{r}^2} + \left(\frac{1}{\overline{r}^{(n)}} + \left(\frac{1}{\overline{D}_{\varkappa\varkappa}^{(n)}}\right)\frac{\mathrm{d}\overline{D}_{\varkappa\varkappa}}{\mathrm{d}\overline{r}}\bigg|_{t=t_n}\right)\frac{\mathrm{d}\overline{c}^{(n+1)}}{\mathrm{d}\overline{r}} - \frac{\overline{c}^{(n+1)}}{\overline{D}_{\varkappa\varkappa}^{(n)}\Delta t} &= 2\overline{\omega}\left(\overline{\Psi}_1^{(n)}\right)^2 \\ + \overline{\omega}\left(\overline{\Psi}_1^{(n)}\right)^2\frac{\overline{r}^{(n)}}{\overline{D}_{\varkappa\varkappa}^{(n)}}\left(\frac{\mathrm{d}\overline{D}_{\varkappa\varkappa}}{\mathrm{d}\overline{r}}\bigg|_{t=t_n}\right) - \frac{\overline{c}^{(n)}}{\overline{D}_{\varkappa\varkappa}^{(n)}\Delta t}\end{aligned} \tag{6.62}$$

$$\begin{aligned}\frac{\mathrm{d}^2\overline{\vartheta}^{(n+1)}}{\mathrm{d}\overline{r}^2} + \left(\frac{1}{\overline{r}^{(n)}} + \left(\frac{1}{\overline{D}_{\vartheta\vartheta}^{(n)}}\right)\frac{\mathrm{d}\overline{D}_{\vartheta\vartheta}}{\mathrm{d}\overline{r}}\bigg|_{t=t_n}\right)\frac{\mathrm{d}\overline{\vartheta}^{(n+1)}}{d\overline{r}} - \frac{\overline{\vartheta}^{(n)}\overline{\vartheta}^{(n+1)}}{\overline{D}_{\vartheta\vartheta}^{(n)}\Delta t} &= -\frac{\overline{\tau}\overline{D}_{\varkappa\varkappa}^{(n)}}{\overline{D}_{\vartheta\vartheta}^{(n)}}\left(\frac{\mathrm{d}\overline{c}}{d\overline{r}}\bigg|_{t=t_n}\right)^2 - \frac{\left(\overline{\vartheta}^{(n)}\right)^2}{\overline{D}_{\vartheta\vartheta}^{(n)}\Delta t} \\ + \frac{2\overline{\tau}\overline{\omega}\overline{D}_{\varkappa\varkappa}^{(n)}}{\overline{D}_{\vartheta\vartheta}^{(n)}}\overline{r}^{(n)}\left(\overline{\Psi}_1^{(n)}\right)^2\frac{\mathrm{d}\overline{c}}{d\overline{r}}\bigg|_{t=t_n} - \frac{\overline{\tau}\overline{D}_{\varkappa\varkappa}^{(n)}\overline{\omega}^2}{\overline{D}_{\vartheta\vartheta}^{(n)}}\left(\overline{r}^{(n)}\right)^2\left(\overline{\Psi}_1^{(n)}\right)^4\end{aligned} \tag{6.63}$$

The boundary conditions for diffusion and thermal subproblems are the same as that of the previous boundary value problems.

The following non-dimensional parameters are assumed in the numerical simulations:

$$\begin{aligned}&\overline{R}_o = 1,\ \overline{R}_i = 0.5,\ \Delta\overline{t} = 0.1,\ \overline{t} = 2,\ \overline{\omega} = 0.05,\ \overline{\tau} = 0.8,\ \overline{\mu}_0 = 1,\ \overline{\mu}_1 = 0.5,\ \overline{\mu}_2 = 0.2, \\ &\overline{D}_0 = 1,\ \overline{D}_T = 1.5,\ \overline{D}_S = 1.2,\ \eta_T = \eta_S = 0.1,\ E_{\mathrm{ref}T} = E_{\mathrm{ref}S} = 1,\ \overline{K}_0 = 1,\ \delta = 10\end{aligned} \tag{6.64}$$

The numerical results are shown in Figs. 18 and 19, which reveals the following important conclusions on the overall behavior of degrading structural members under torsional shear:

1. The numerical results in Fig. 18 reveal that there is relaxation of moment for fixed deformation. In addition, the twisting moment required to maintain a fixed angle of twist decreases with increase in $\overline{\mu}_1$. Similar type of behavior is observed when $\overline{\mu}_1$ is kept constant and $\overline{\mu}_2$ is varied.

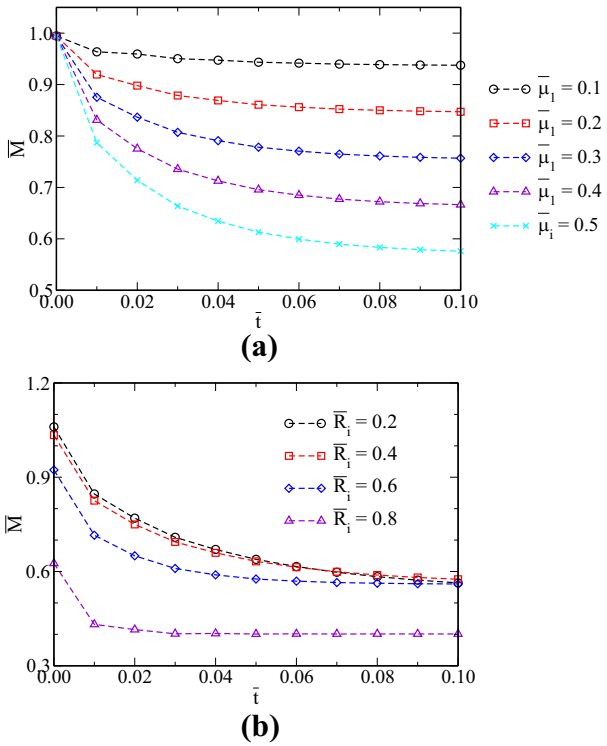

Fig. 18 Torsional shear of a degrading cylinder: This figure shows the twisting moment at various instants of time due to a given angle of twist per unit length of the cylinder, $\overline{\Psi}_1 = 0.75$. One can see that as $\overline{\mu}_1$ increases the twisting moment required to keep $\overline{\Psi}_1$ unchanged, decreases. Similar type of behavior is observed when $\overline{\mu}_1$ is kept constant and $\overline{\mu}_2$ is varied. *Herein, the main observation is that moment relaxation not only depends on material degradation but also on the geometry of the degrading body*. **a** Moment under different $\overline{\mu}_1$, **b** moment under different $\overline{R}_i$

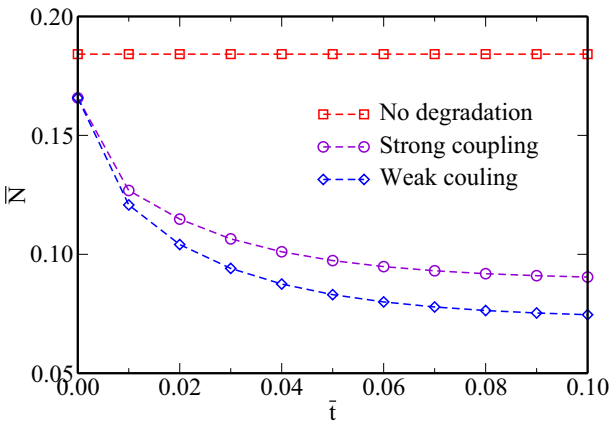

Fig. 19 Torsional shear of a degrading cylinder: This figure shows the non-dimensionalized normal force $\overline{N}$ due to Poynting effect at various instants of time. Analysis is performed for a given angle of twist per unit length of the cylinder, $\overline{\Psi}_1 = 0.75$. When there is no degradation, the normal force is constant. However, due to degradation one can see that the normal force relaxes over time. The decrease in this normal force for weak coupling is higher than that for the strong coupling

2. In Fig. 18, we also observe moment relaxation due to material degradation when both the transport and thermal subproblems are close to steady states. Moreover, one can see that moment relaxation depends on the geometry of the specimen. These aspects differentiate the stress relaxation due to degradation from the stress relaxation due to viscoelasticity.
3. We observe that the normal force due to Poynting effect is decreasing over time as a result of degradation, see Fig. 19. Without degradation, the normal force is a constant (which is the case for hyperelastic materials).

7 Concluding remarks

This paper has made several contributions to the modeling of degradation of materials due to the presence of an adverse chemical species and temperature. *First*, a consistent mathematical model has been derived that has firm continuum thermodynamics underpinning. The constitutive relations, which give rise to coupled deformation–thermal transport equations, have been derived by appealing to the maximization of the rate of dissipation, which is a stronger version of the second law of thermodynamics. The proposed model is hierarchical in the sense that it recovers many existing models as special cases. *Second*, the materials parameters have been calibrated with an experimental data set available in the literature. *Third*, it has been shown that the unsteady solutions to the proposed degradation model are bounded and stable in the sense of Lyapunov even under large deformations and large strains. *Last but not the least*, using several canonical problems in degradation mechanics, we illustrated the effects of chemical degradation and thermal degradation on the response of a body that is initially hyperelastic. Some of the main features of degradation and of the proposed model can be summarized as follows:

(C1) Degradation introduces spatial inhomogeneity. That is, a material which is originally homogeneous may cease to be homogeneous due to degradation.
(C2) The proposed mathematical model can provide the variation of important quantities like chemical potential within the body, which is essential in incorporating chemical reactions into the modeling. Of course, one needs to provide other essential information (e.g., stoichiometry, law of mass action, dissipation due to chemical reactions, reaction rates, exothermic vs. endothermic energy changes) to incorporate chemical reactions.
(C3) In a coupled chemo–thermo–mechano degradation problem, for instance degrading shell problem, thermo-mechanical coupling plays a vital role in evaluating extent of damage and pressure loading. For thermo-dominated problem, healing-like behavior is observed at early time steps. This is because of the deformation-dependent thermal diffusivity. However, this healing-like behavior becomes less distinct (or does not even exist) when the chemo-degradation achieves the dominance (see Fig. 10).
(C4) The extent of damage in a structural member can be both qualitatively and quantitatively different under strong and weak couplings between mechanical, thermal, and transport processes. More importantly, weak coupling may overpredict the material degradation in some cases, while in other cases it may underpredict the degradation. It is, therefore, of paramount importance to select the extent of coupling between the mechanical, thermal, and chemical processes.
(C5) The usual assumptions on either kinematics or stresses, which may be justified for non-degrading members, may no longer hold under degradation. For example, assumptions on the location of neutral axis or the location of the maximum stress on the outer fibers in beam bending will not hold under degradation.
(C6) Degrading structural members may exhibit some responses that are typically associated with viscoelasticity. In particular, we have shown that degradation can induce stress relaxation and creep in the response of the materials even in the case of finite-sized bodies. In contrast to a viscoelastic body (which creeps continuously upon the application of a load), the body undergoing chemical degradation ceases to creep for practical purposes after a certain period of time. This the moment when the transport of chemical species is close to a steady state, if there is no volumetric source and the boundary conditions are unchanged over time. A similar trend holds even in the case of thermal degradation. This characteristic behavior of degrading solids can be used to differentiate the creep associated with viscoelasticity and degradation. Moreover, stress relaxation due to degradation depends on the geometry of the specimen, which is also different from the case due to viscoelasticity.

A possible future research work can be toward incorporating fatigue and fracture into the degradation modeling. A related scientific question can be toward addressing the effect of material degradation on the crack initiation and its propagation.

Acknowledgments The authors acknowledge the support from the Department of Energy through Nuclear Energy University Programs (NEUP). The opinions expressed in this paper are those of the authors and do not necessarily reflect that of the sponsor(s).

References

1. ABAQUS/CAE/Standard, Version 6.14-1. Simulia, Providence. www.simulia.com (2014)
2. Adler, S.B.: Chemical expansivity of electrochemical ceramics. J. Am. Ceram. Soc. **84**, 2117–2119 (2001)

3. Allam, S.M., Elbakry, H.M.F., Rabeai, A.G.: Behavior of one-way reinforced concrete slabs subjected to fire. Alex. Eng. J. **52**, 749–761 (2013)
4. ANSYS Multiphysics, Version 16.0. ANSYS, Inc., Canonsburg. www.ansys.com (2015)
5. Antman, S.S.: Nonlinear Problems of Elasticity. Springer, New York (1995)
6. Batchelor, A.W., Lam, L.N., Chandrasekaran, M.: Materials Degradation and Its Control by Surface Engineering, 3rd edn. Imperial College Press, London (2003)
7. Bhowmick, S., Shenoy, V.B.: Effect of strain on the thermal conductivity of solids. J. Chem. Phys. **125**, 164513 (2006)
8. Björk, F., Eriksson, C.A., Karlsson, S., Khabbaz, F.: Degradation of components in flooring systems in humid and alkaline environments. Constr. Build. Mater. **17**, 213–221 (2003)
9. Blond, E., Richet, N.: Thermomechanical modelling of ion-conducting membrane for oxygen separation. J. Eur. Ceram. Soc. **28**, 793–801 (2008)
10. Bouadi, H., Sun, C.T.: Hygrothermal effects on the stress field of laminated composites. J. Reinf. Plast. Compos. **8**, 40–54 (1989)
11. Bouadi, H., Sun, C.T.: Hygrothermal effects on structural stiffness and structural damping of laminated composites. J. Mater. Sci. **25**, 499–505 (1990)
12. Bowen, R.M.: Theory of mixtures. In: Eringen, A.C. (ed.) Continuum Physics, vol. III. Academic Press, New York (1976)
13. Buonsanti, M., Leonard, G., Scoppelliti, F.: Equilibrium state of a binary granular solids mixture. Appl. Mech. Mater. **52**, 389–392 (2011)
14. Cai, L.W., Weitsman, Y.J.: Non-Fickian moisture diffusion in polymeric composites. J. Compos. Mater. **28**, 130–154 (1994)
15. Černy, R., Rovnaníková, P.: Transport Processes in Concrete. CRC Press, New York (2002)
16. Cho, D.W., Kim, K.: The mechanisms of moisture damage in asphalt pavement by applying chemistry aspects. KSCE J. Civ. Eng. **14**, 333–341 (2010)
17. Coleman, B.D., Dill, E.H.: On thermodynamics and the stability of motions of materials with memory. Arch. Ration. Mech. Anal. **51**, 1–53 (1973)
18. COMSOL Multiphysics User's Guide, Version 5.0-1. COMSOL, Inc., Burlington. www.comsol.com (2014)
19. Coussy, O.: Poromechanics. John Wiley & Sons Inc, New York (2004)
20. Criscione, J.C., Humphrey, J.D., Douglas, A.S., Hunter, W.C.: An invariant basis for natural strain which yields orthogonal stress response terms in isotropic hyperelasticity. J. Mech. Phys. Solids **48**, 2445–2465 (2000)
21. Darbha, S., Rajagopal, K.R.: Unsteady motions of degrading or aging linearized elastic solids. Int. J. Non Linear Mech. **44**, 478–485 (2009)
22. Dym, C.L.: Stability Theory and Its Applications to Structural Mechanics. Dover Publications, New York (2002)
23. Ericksen, J.L.: Thermoelastic stability. In: Proceedings of the 5th US National Congress of Applied Mechanics, pp. 187–193 (1966)
24. Farrar, C.R., Worden, K.: Structural Health Monitoring: A Machine Learning Perspective. Wiley, West Sussex (2013)
25. Gawin, D., Pesavento, F., Schrefler, B.A.: Modeling deterioration of cementitious materials exposed to calcium leaching in non-isothermal conditions. Comput. Methods Appl. Mech. Eng. **198**, 3051–3083 (2009)
26. Glasser, F.P., Marchand, J., Samson, E.: Durability of concrete degradation phenomena involving detrimental chemical reactions. Cem. Concr. Res. **38**, 226–246 (2008)
27. Grasberger, S., Meschke, G.: Thermo-hygro-mechanical degradation of concrete: from coupled 3D material modeling to durability-oriented multifield structural analyses. Mater. Struct. **37**, 244–256 (2004)
28. Gros, X.E.: NDT Data Fusion. Wiley, London (1997)
29. Gu, J.D., Ford, T.E., Berke, N.S., Mitchell, R.: Biodeterioration of concrete by the fungus Fusarium. Int. Biodeterior. Biodegrad. **41**, 101–109 (1998)
30. Gurtin, M.E.: Thermodynamics and stability. Arch. Ration. Mech. Anal. **59**, 53–96 (1975)
31. Hale, J.K., Kocak, H.: Dynamics and Bifurcations. Springer, New York (1991)
32. Harper, C.A.: Handbook of Plastics, Elastomers, & Composites, 4th edn. McGraw-Hill, New York (2002)
33. Heath, M.T.: Scientific Computing—An Introductory Survey, 2nd edn. McGraw-Hill, New York (2005)
34. Herrmann, A.W.: ASCE 2013 Report Card for America's Infrastructure. In: IABSE Symposium Report, vol. 99, pp. 9–10. International Association for Bridge and Structural Engineering (2013)
35. Holzapfel, G.A.: Nonlinear Solid Mechanics. Wiley, Chichester (2000)
36. Jarkova, E., Pleiner, H., Müller, H.W., Fink, A., Brand, H.R.: Hydrodynamics of nematic ferrofluids. Eur. Phys. J. E **5**, 583–588 (2001)
37. Jung, Y.G., Peterson, I.M., Kim, D.K., Lawn, B.R.: Lifetime-limiting strength degradation from contact fatigue in dental ceramics. J. Dent. Res. **79**, 722–731 (2000)
38. Kachanov, L.: Introduction to Continuum Damage Mechanics. Springer, Dordrecht (1986)
39. Kaplan, M.F.: Concrete Radiation Shielding: Nuclear Physics, Concrete Properties, Design and Construction. Wiley, New York (1989)
40. Karra, S., Rajagopal, K.R.: Degradation and healing in a generalized neo-Hookean solid due to infusion of a fluid. Mech. Time-Depend. Mater. **16**, 85–104 (2012)
41. Klepach, D., Zohdi, T.I.: Strain assisted diffusion: modeling and simulation of deformation-dependent diffusion in composite media. Compos. Part B Eng. **56**, 413–423 (2014)
42. Kolberg, R., Wineman, A.: Response of beams of non-linear viscoelastic materials exhibiting strain-dependent stress relaxation. Int. J. Non Linear Mech. **32**, 863–883 (1997)
43. Lai, W.M., Hou, J.S., Mow, V.C.: A triphasic theory for the swelling and deformation behaviors of articular cartilage. J. Biomech. Eng. **113**, 245–258 (1991)
44. Lemaitre, J., Desmorat, R.: Engineering Damage Mechanics: Ductile, Creep, Fatigue and Brittle Failures. Springer, Berlin (2005)
45. Li, V.C.: On engineered cementitious composites (ECC). J. Adv. Concr. Technol. **1**, 215–230 (2006)

46. Lurie, A.I.: Nonlinear Theory of Elasticity, North Holland Series in Applied Mathematics and Mechanics. Elsevier Science, Amsterdam (1990)
47. MATLAB: The MathWorks Inc. Natick, Massachusetts (2012)
48. Maugin, G.A.: The Thermomechanics of Nonlinear Irreversible Behaviours: An Introduction. World Scientific Publishing Company, New Jersey (1998)
49. McAfee, K.B.: Stress-enhanced diffusion in glass I. Glass under tension and compression. J. Chem. Phys. **28**, 218–226 (1958a)
50. McAfee, K.B.: Stress-enhanced diffusion in glass II. Glass under shear. J. Chem. Phys. **28**, 226–229 (1958b)
51. Morozovska, A.N., Eliseev, E.A., Tagantsev, A.K., Bravina, S.L., Chen, L.Q., Kalinin, S.V.: Thermodynamics of electromechanically coupled mixed ionic–electronic conductors: deformation potential, Vegard strains, and flexoelectric effect. Phys. Rev. B **83**, 195313 (2011)
52. Mudunuru, M.K., Nakshatrala, K.B.: A framework for coupled deformation–diffusion analysis with application to degradation/healing. Int. J. Numer. Methods Eng. **89**, 1144–1170 (2012)
53. Muliana, A., Rajagopal, K.R., Subramanian, S.C.: Degradation of an elastic composite cylinder due to the diffusion of a fluid. J. Compos. Mater. **43**, 1225–1249 (2009)
54. Myers, E.R., Lai, W.M., Mow, V.C.: A continuum theory and an experiment for the ion-induced swelling behavior of articular cartilage. J. Biomech. Eng. **106**, 151–158 (1984)
55. Naus, D.J.: Primer on durability of nuclear power plant reinforced concrete structures—a review of pertinent factors. Technical report, Oak Ridge National Laboratory (ORNL), NUREG/CR–6927 (2007)
56. Ogden, R.W.: Nonlinear Elastic Deformations. Dover Publications, New York (1997)
57. Onsager, L.: Reciprocal relations in irreversible processes. I. Phys. Rev. **37**, 405 (1931a)
58. Onsager, L.: Reciprocal relations in irreversible processes. II. Phys. Rev. **38**, 2265 (1931b)
59. Peng, S.T., Landel, R.F.: Induced anisotropy of thermal conductivity of polymer solids under large strains. J. Appl. Polym. Sci. **19**, 49–68 (1975)
60. Picard, R., Leis, R.: Some remarks on the horizontal line method. Math. Methods Appl. Sci. **2**, 471–479 (1980)
61. Pierron, F., Grédiac, M.: The Virtual Fields Method: Extracting Constitutive Mechanical Parameters From Full-Field Deformation Measurements. Springer, New York (2009)
62. Plešek, J., Kruisová, A.: Formulation, validation and numerical procedures for Hencky's elasticity model. Comput. Struct. **84**, 1141–1150 (2006)
63. Rajagopal, K.R., Srinivasa, A.R., Wineman, A.S.: On the shear and bending of a degrading polymer beam. Int. J. Plast. **23**, 1618–1636 (2007)
64. Rothe, E.: Zweidimensionale parabolische randwertaufgaben als grenzfall eindimensionaler randwertaufgaben. Math. Ann. **102**, 650–670 (1930)
65. Sadd, M.H.: Elasticity: Theory, Applications, and Numerics, 3rd edn. Academic Press, Oxford (2014)
66. Saltelli, A., Tarantola, S., Campolongo, F., Ratto, M.: Sensitivity Analysis in Practice: A Guide to Assessing Scientific Models. Wiley, West Sussex (2004)
67. Saltelli, A., Ratto, M., Andres, T., Campolongo, F., Cariboni, J., Gatelli, D., Saisana, M., Tarantola, S.: Global Sensitivity Analysis: The Primer. Wiley, West Sussex (2008)
68. Sih, G.C., Michopoulos, J.G., Chou, S.C.: Hygrothermoelasticity. Martinus Nijhoff Publishers, Dordrecht (1986)
69. Springman, R.M., Bassani, J.L.: Mechano-chemical coupling in the adhesion of thin-shell structures. J. Mech. Phys. Solids **57**, 909–931 (2009)
70. Strogatz, S.H.: Nonlinear Dynamics and Chaos: With Applications to Physics, Biology, Chemistry, and Engineering. Westview Press, Cambridge (2001)
71. Sutton, M.A., Orteu, J.J., Schreier, H.W.: Image Correlation for Shape, Motion and Deformation Measurements: Basic Concepts, Theory, and Applications. Springer, New York (2009)
72. Swamy, R.N.: The Alkali-Silica Reaction in Concrete. CRC Press, New York (2002)
73. Ulm, J.F., Coussy, O., Kefei, L., Larive, C.: Thermo-chemo-mechanics of ASR expansion in concrete structures. J. Eng. Mech. **126**, 233–242 (2000)
74. Venerus, D.C., Schieber, J.D., Balasubramanian, V., Bush, K., Smoukov, S.: Anisotropic thermal conduction in a polymer liquid subjected to shear flow. Phys. Rev. Lett. **93**, 098301 (2004)
75. Voyiadjis, G.Z., Kattan, P.I.: Damage Mechanics. CRC Press, Taylor & Francis Group, Boca Raton (2005)
76. Wang, S., Li, V.C.: High-early-strength engineered cementitious composites. ACI Mater. J. **103**, 97–105 (2006)
77. Weitsman, Y.J.: Coupled damage and moisture-transport in fiber-reinforced, polymeric composites. Int. J. Solids Struct. **23**, 1003–1025 (1987)
78. Weitsman, Y.J.: Anomalous fluid sorption in polymeric composites and its relation to fluid-induced damage. Compos. Part A Appl. Sci. Manuf. **37**, 617–623 (2006)
79. Weitsman, Y.J., Guo, Y.J.: A correlation between fluid-induced damage and anomalous fluid sorption in polymeric composites. Compos. Sci. Technol. **62**, 889–908 (2002)
80. Wiggins, S.: Introduction to Applied Nonlinear Dynamical Systems and Chaos, 2nd edn. Springer, New York (2003)
81. Willam, K., Rhee, I., Xi, Y.: Thermal degradation of heterogeneous concrete materials. J. Mater. Civ. Eng. **17**, 276–285 (2005)
82. Zheng, R., Tanner, R.I., Fan, X.J.: Injection Molding: Integration of Theory and Modeling Methods. Springer, Berlin (2011)
83. Ziegler, H.: An Introduction to Thermomechanics. North Holland Publishing Company, Amsterdam (1983)